STIM1 R304W causes muscle degeneration and impaired platelet activation in mice

Thilini H. Gamage[a], Gjermund Gunnes[b], Robert Hugh Lee[c], William Edward Louch[d], Asbjørn Holmgren[a], Joseph D. Bruton[e], Emma Lengle[a], Terje R. Selnes Kolstad[d], Tobias Revold[b], Silja Svanstrøm Amundsen[a], Knut Tomas Dalen[f], Pål Andre Holme[g,h], Geir Erland Tjønnfjord[g,h], Geir Christensen[d], Håkan Westerblad[e], Arne Klungland[i], Wolfgang Bergmeier[c], Doriana Misceo[a,*], Eirik Frengen[a,*]

[a]Department of Medical Genetics, Oslo University Hospital and University of Oslo, Oslo, Norway

[b]Faculty of Veterinary Medicine, Norwegian University of Life Sciences, Norway

[c]Department of Biochemistry and Biophysics, University of North Carolina, Chapel Hill, USA

[d]Institute for Experimental Medical Research, Oslo University Hospital and University of Oslo Norway

[e]Department of Physiology and Pharmacology, Karolinska Institute, 171 77 Stockholm, Sweden.

[f]Norwegian Transgenic Center, University of Oslo, Oslo, Norway

[g]Department of Haematology, Oslo University Hospital, Norway

[h]Institute of Clinical Medicine, University of Oslo, Oslo, Norway

[i]Department of Molecular Medicine, Oslo University Hospital, Norway

[*] These authors contributed equally to this work.

Correspondence:

Eirik Frengen

Department of Medical Genetics, University of Oslo, Norway

E-mail: eirik.frengen@medisin.uio.no

Keywords:

Stim1 R304W; muscle degeneration; Stormorken syndrome; Stim1 expression; Platelet dysfunction

Abstract

STIM1 and ORAI1 regulate store-operated Ca^{2+} entry (SOCE) in most cell types, and mutations in these proteins have deleterious and diverse effects. We established a mouse line expressing the STIM1 R304W gain-of-function mutation causing Stormorken syndrome to explore effects on organ and cell physiology. While STIM1 R304W was lethal in the homozygous state, surviving mice presented with reduced growth, skeletal muscle degeneration, and reduced exercise endurance. Variable STIM1 expression levels between tissues directly impacted cellular SOCE capacity. In contrast to patients with Stormorken syndrome, STIM1 was downregulated in fibroblasts from $Stim1^{R304W/R304W}$ mice, which maintained SOCE despite constitutive protein activity. In studies using foetal liver chimeras, STIM1 protein was undetectable in homozygous megakaryocytes and platelets, resulting in impaired platelet activation and absent SOCE. These data indicate that downregulation of STIM1 R304W effectively opposes the gain-of-function phenotype associated with this mutation, and highlight the importance of STIM1 in skeletal muscle development and integrity.

Introduction

Stromal interaction molecule 1 (STIM1) is an endoplasmic reticulum (ER) resident transmembrane protein able to sense Ca^{2+} levels in the ER, the main Ca^{2+} repository in most cells. The STIM1 N-terminal region is located in the ER lumen, and is separated from the cytosolic C-terminal region by a transmembrane domain. The STIM1 C-terminal interacts with the plasma membrane (PM) resident calcium release-activated calcium modulator 1, ORAI1. A decrease in ER Ca^{2+} levels is sensed by the EF-hand domain in the STIM1 N-terminal, resulting in its activation, oligomerisation, and finally lateral translocation in the ER membrane. STIM1 interacts with ORAI1 through a coiled coil domain (CC), forming STIM1-ORAI1 puncta at ER-PM junctions [1-2]. Thus, binding of STIM1 activates ORAI1, the pore forming subunit of calcium release activated Ca^{2+} (CRAC) channel, allowing Ca^{2+} influx. This mechanism is known as store operated calcium entry (SOCE) [3-5]. STIM1 and ORAI1 together facilitate SOCE in both excitable and non-excitable cells, providing a key mechanism for cellular Ca^{2+} influx [6-7].

Mutations in *ORAI1* or *STIM1* have been shown to cause five Mendelian diseases in humans [5, 8-12]. Both biallelic loss of function (LoF) mutations and heterozygous gain of function (GoF) mutations are pathogenic. Biallelic LoF mutations in *STIM1* or *ORAI1* result in absence of SOCE and patients present with Immunodeficiency 10 (IMD10, OMIM #612783) or Immunodeficiency 9 (IMD9, OMIM #612782) [7, 11]. In mice, global knockout (KO) of *Stim1* or *Orai1* results in homozygous lethality. Indeed, sixty to seventy percent of homozygous *Stim1* or *Orai1* KO pups were observed to die within a few hours of birth, while remaining animals exhibited significant growth retardation and increased mortality within the first 4 weeks of life due to muscle weakness or respiratory failure [7, 13-15].

GoF mutations in *ORAI1* or in the *STIM1* EF-hand domain result in constitutively active SOCE and cause tubular aggregate myopathy 1 or 2 in patients (TAM1, OMIM #160565, TAM2, OMIM #615883) [8, 10, 16]. One mouse model expressing the GoF STIM1 EF-hand mutation D84G (the $Stim1^{Sax}$ mice) has been described [17]. In contrast to patients carrying the same mutation and presenting with TAM1, the heterozygous $Stim1^{Sax}$ mice showed macro-thrombocytopenia and a bleeding disorder. This haematological dysfunction was more severe in the homozygous $Stim1^{Sax}$ mice, which died *in utero* [17]. No muscular defect has been described in the $Stim1^{Sax}$ mice [17].

Another *STIM1* GoF mutation, R304W, is located in the STIM1 coiled-coil 1 (CC1) domain and has been previously shown to result in constitutively active SOCE [9, 12, 18], causing Stormorken syndrome (STRMK, OMIM #185070). The syndrome manifests with a skeletal muscle phenotype (including tubular aggregate myopathy, muscle spasms and weakness, lack of endurance, and increased serum creatine kinase levels) and a haematological phenotype (including mild anaemia and

mild bleeding disorder related to thrombocytopathy and thrombocytopenia). The syndrome also manifests miosis, ichthyosis, and asplenia [9, 12, 18-20]. Although GoF mutations in the CC1 domain typically cause the complex Stormorken syndrome, three patients expressing the STIM1 R304Q mutation presented with myalgia and only a single patient exhibited thrombocytopenia [21]. Thus, TAM1 and Stormorken syndrome may be described as part of a clinical continuum, with overlapping manifestations of STIM1 GoF mutations [19, 21].

Due to the diverse and complex phenotype caused by STIM1 R304W in humans we studied its effect on cellular Ca^{2+} handling and its phenotypic consequences in a Stim1 R304W knock-in mouse model with focus on skeletal muscle and platelets. We found that the mutation caused constitutive STIM1 activation and cell and species specific regulation of the mutant STIM1 expression resulting in muscle degradation and platelet dysfunction.

Methods

Establishment *Stim1* ^{R304W} mice

The mouse model carrying the *Stim1* (NC_000073.6) Chr7:102421471A>T (GRCm38.p4) mutation was established using CompoZr^{TM} custom Zinc Finger Nuclease (ZFN) technology (Sigma Aldrich, Missouri, USA) combined with a repair fragment to stimulate homology directed repair (HDR) at the target loci. The Fok-I based DNA binding heterodimeric ZFN pair was custom designed to bind and cleave ~20 bp upstream of the *Stim1* target site; 5'-ACCTTGCCAAGCaggaagcTCAGCGGCTGAAGGAGCT-3' (the ZFN binding sequence in uppercase and the nuclease Fok1 recognition sequence in lowercase). To introduce the mutation, ~1600 dsDNA fragment containing the A>T substitution at the center was synthesized and sequence verified (Genewix Inc., South Plainfield, NJ, USA). Three to four week old female B6CBAF1/JRj mice (Janvier, France) were superovulated by injecting 5 IU pregnant mares' serum (PMS, Sigma Aldrich) followed by a second injection 45 hours later with 5 IU of human chorionic gonadotropin (HCG, Sigma Aldrich). Superovulated females were subsequently mated with C57BL/6NTac males (Taconic, Ejby, Denmark) and fertilized embryos were collected from oviducts the next morning. The ZFN pair (1 ng/μl) and the repair template (2 or 3 ng/μl) were diluted in EmbryoMax Injection buffer (Speciality media, Sigma Aldrich) and co-injected into zygotes. Injected zygotes were cultured in KSOM (Merck Millipore, Burlington, MA, USA) at 37°C at 5 % CO_2 until implanted later the same day. Pseudo-pregnant CD1 (Envigo, The Netherlands) foster mothers were generated by mating with vasectomized CD1 males. Ear biopsies for identification of founders were taken at weaning.

Maintenance of mice

All animals were housed under standard conditions (12:12-hr light/dark, 21±2°C temperature and 55±5% relative humidity) with *ad libitum* access to water and standard chow. Mice were weighed weekly to monitor their growth. All animal experimental protocols for generation, breeding and use of transgenic animals in Norway were registered and approved by the Norwegian Food Safety Authority (Mattilsynet, Experimental animal welfare supervision and application system ID 7216 and 6991) and followed the ethical guidelines given in Directive 2010/63/EU of the European Parliament on the protection of animals used for scientific purposes. The procedures conducted at the University of North Carolina, USA were approved by The University of North Carolina at Chapel Hill Institutional Animal Care and Use Committee (IACUC).

Identification and genotyping of Stim1 ^{R304W} mice

Offspring following ZFN modifications were screened for the genomic insertion of the ZFN cassette using Platinum™ Taq DNA Polymerase High Fidelity (Invitrogen, CA, USA) and primers Stim1-F1 and Stim1-R1, followed by Sanger sequencing (BigDye™ Terminator v3.1 Cycle Sequencing Kit, Applied Biosystems, CA, USA) (primer sequences listed in the Supplementary table 1). Animals positive for *Stim1* (NC_000073.6) chr7:102421471A>T (GRCm38.p4) were then selected to determine if the mutation was specifically targeted into the *Stim1* gene in the mice. A PCR fragment of 2166 bp covering the complete ZFN cassette was amplified with long range PCR (TaKaRa LA DNA polymerase, Takara Bio USA, Inc., CA, USA) using primers: Stim1-F2 and Stim1-R2 upstream and downstream of the ZFN cassette flanking the gene (Supplementary Table 1). Sanger sequencing of the complete fragment was performed using the primers designed along the length of the fragment; Stim1-F3, Stim1-R3, Stim1-F4, Stim1-R4, Stim1-R6 (Supplementary Table 1). All animals negative for the A>T substitution at the target site and/or with additional mutations detected in the cassette were excluded. The 2166 bp PCR-fragments from the remaining animals were cloned by TOPO TA cloning according to the manufacturer's instructions (TOPO TA cloning kit for sequencing, Invitrogen). Sanger sequencing of 10 independent clones from the founder animal showed only the Stim1 mutation at Chr7:102421471bp (A>T) and no additional modifications in the same allele. The sequence reads were assembled using Sequencing Analysis software v5.2 (Applied Biosystems) and aligned with the mouse reference genome in the UCSC genome browser (Mouse Dec. 2011 (GRCm38/mm10) Assembly) and MEGA4 software [22]. The mouse line described here is referred to as Stim1^{R304W} and originated from one founder female backcrossed to C57bl/6J male mouse (Envigo) and further intercrossed to establish the Stim1 R304W colony.

Whole genome sequencing of the Stim1^{R304W} female founder mouse

Whole genome sequencing (WGS) of the female founder mouse DNA was performed (Novogene, China). In brief, reads passing quality filters were mapped to the GRCm38.p4 reference genome using the BWA-MEM algorithm [23] . SAMtools was used to remove duplicates and to sort the reads in the resulting bam file [24]. Metrics and statistics of coverage and depth were collected with Picard version 2.12.1 (Broad Institute, Cambridge, MA, USA). For the detection of any structural variation caused by transgene integration, paired-end reads and split-read based variant calling analysis were performed with the software DELLY [25] and Breakdancer [26]. SNP and InDel variations were detected by SAMtools mpileup [27] . The high confidence integration sites reported by variant calling were extracted and further checked as visualized by The Integrative Genomics Viewer (IGV) [28], and the copy number of each transgene was assumed by their effective depth relative to the genome-wide sequencing depth. A total of 779337818 reads were obtained with a 99.28% mapping rate. The whole genome coverage was 91% ≥1x, 90.1% ≥ 5x and 88% ≥ 15x.

Material from patients with Stormorken syndrome and healthy controls

Cultured skin derived fibroblast cells and whole blood samples from two patients with Stormorken syndrome (F1 III-1 and F2 II-3 in Misceo. et al 2014) were obtained [9]. Similarly derived, fibroblast cell cultures from two healthy individuals were used as controls for SOCE experiments. Blood samples from two healthy individuals were used as controls for platelet-protein preparation. All samples were obtained following informed consent.

Real time qPCR of *Stim1* cDNA

RNA was harvested from whole blood in PAX-solution as described previously [29]. RNA concentration was measured with Qubit nanodrop RNA high sensitivity (Thermo Fischer Scientific, Waltham, MA, USA), and quality assessed with Agilent BioAnalyzer RNA Nano (Agilent Technologies, Waldbronn, Germany). Samples with RIN values below 7 were excluded from experiment. cDNA was synthesized from 0.25-1µg RNA using High-Capacity cDNA Reverse Transcription Kit (Applied Biosystems).

qPCR was run in an QuantStudio 12k instrument, using manufacturers software and instructions (Thermo Fischer). SYBR® Green JumpStart™ Taq ReadyMix™ (Sigma Aldrich) was used for the amplification of cDNA with *Stim1* specific primers; Stim1_cDNA_F, Stim1_cDNA_R (Supplementary Table 1). All primer pairs were tested for efficiency with a 5-point dilution series, and melt curve analysis was used to confirm the presence of a single amplicon for each reaction. Data was analysed by normalizing against three reference genes; Rplp0, Ppib and Eef2 (Supplementary Table 1).

Examination of mouse embryos

Mouse embryos collected at 12.5, 13.5, 14.5, 15.5, 16.5 and 17dpc were evaluated macroscopically for gross abnormalities and signs of bleeding. A blood sample was collected for quantification of platelets and tail biopsies were collected for genotyping and gender determination. Embryos at 14.5 and 16.5dpc were fixed, paraffin embedded and sectioned across the midline to obtain whole mount sections of the embryo and stained with Hematoxylin and eosin (HE). Following deparaffinization and antigen retrieval according to the manufacturer's instructions, sections from 14.5 and 16.5dpc embryos were immuno-stained with an antibody binding the STIM1 N-terminal (LS-B10807-50, LS-Bio Inc., Seattle, WA, USA). The anti-rabbit IgG-Alexa 488 (Thermo Fischer Scientific) was used as secondary antibody to detect and visualise STIM1 and evaluate the expression in embryonic tissues.

Whole cell measurements of Ca^{2+} concentration and SOCE in cultured mouse neonatal fibroblast cells

Fibroblasts were grown from skin biopsies harvested from 0-2 days old mice in 10% FBS and 10 mM PenStrep supplemented DMEM media (Gibco, Thermo Fischer Scientific). Cells were harvested after two weeks and plated on glass coverslips coated with gelatin-fibronectin and incubated overnight at 37^0C supplemented with 5% CO_2. The fibroblast-containing coverslips were then loaded with Ca^{2+} measuring dyes, Indo-1-AM (Molecular probes/Invitrogen, Carlsbad, CA, USA) or Fluo-4-AM (Molecular probes/Invitrogen) for 20 and 15 minutes, respectively, and the experiments were conducted as previously described [9]. Indo-1-AM loaded cells were superfused with Hepes Tyrode (HT) buffer (140 mM NaCl, 0.5 mM $MgCl_2$, 5.0 mM HEPES, 5.5 mM glucose, 0.4 mM NaH_2PO_4, 5.4 mM KCl, pH 7.4 at 37°C) containing 2 mM Ca^{2+} and whole cell fluorescence was measured. The corresponding resting $[Ca^{2+}]_i$ was calculated as described previously [9]. For assessment of SOCE, Ca^{2+} stores were first depleted by application of the SERCA inhibitor thapsigargin (2 µM, Sigma Aldrich) in the presence of Ca^{2+}-free HT for 5 min, followed by rapid reintroduction of 10 mM Ca^{2+}. SOCE was calculated as the resulting increase in fluorescence intensity, and calibrated to $[Ca^{2+}]$ as previously described [9]..

Transfection of NIH 3T3 cells

NIH 3T3 mouse embryonic fibroblast cell line (Sigma Aldrich) was grown in DMEM with high glucose (4500 mg/L) (Sigma Aldrich), supplemented with 10% Bovine Calf Serum (BCS, Thermo Fisher Scientific), 2% PenStrep (Thermo Fisher Scientific) and 2mM L-glutamine (Thermo Fisher Scientific). The cells were seeded on glass coverslips in a 6 well plate coated with gelatin-fibronectin and incubated overnight prior to transfection with Polyjet transfection reagent (SignaGen Laboratories, MD, USA). Vectors expressing mouse STIM1_WT-YFP or STIM1_R304W-YFP [12] (kind gift from Dr. Leonidas Tsiokas, University of Oklahoma Health Sciences Centre, USA) were transfected with a

vector expressing mouse Orai1 in a 1:1 ratio (kind gift from Dr. Stefan Feske, New York University Medical Centre, USA). Cells were imaged at 24 hours post-transfection using Zeiss LSM 800 with Airyscan (ZEISS microscopy, Oberkochen, Germany) microscope and with ZEN imaging software (ZEISS microscopy). Images were analysed to measure the intensity of YFP signals using Fiji image processing software [30]. Raw images were cropped to remove any debris or secondary cells in the field of view and analysed with a macro which used contrast enhancement, background subtraction, blurring and binarization. Regions of interest identified by elevated fluorescent signals were analysed to determine the number and intensity of STIM1 aggregates.

Western blotting

Whole cell protein lysates were prepared from primary fibroblasts and NIH 3T3 cells using 1x RIPA buffer (Sigma Aldrich). Cells were washed twice with 1x PBS, pH 7.4 (Gibco, Life technologies) and the cell pellet was lysed with 1x RIPA buffer supplemented with Protease and Phosphatase inhibitor cocktail (Thermo Fischer Scientific) for 15 minutes at 4°C followed by centrifugation at 13000 rpm for 15 minutes at 4°C.

Tissue lysates from snap frozen skeletal muscle samples were made with 1x RIPA buffer using gentleMACS™ Octo Dissociator (Miltenyi Biotec, Germany). Lysates were centrifuged at 13000 rpm for 15 minutes at 4°C and supernatant stored at -80^{0}C until use.

Protein concentrations were measured with Pierce BCA Protein Assay kit according to manufacturer's instructions (Thermo Fischer Scientific). Protein lysates from washed platelets (described in flowcytometry studies on platelets section) were prepared using 2x RIPA buffer. All western blots were performed according to standard protocols using Mini-PROTEAN TGX Stain-Free Precast Gels and apparatus (Bio-rad Laboratories, CA, USA). List of the antibodies used is provided in Supplementary Table 2.

Necropsy

A full necropsy was performed on eight mice per genotype in Stim1$^{+/+}$ and Stim1$^{R304W/+}$ and three Stim1$^{R304W/R304W}$ mice euthanized at 5-6 months age. Tissues were harvested and snap frozen and/or fixed in 10% neutral buffered formalin. Blood samples were collected by cardiac puncture to measure blood cell counts, total Ca^{2+}, total protein, haemoglobin and albumin.

Histological staining of formalin-fixed tissue sections was performed according to routine protocols. A standard examination for muscle degeneration parameters were done on HE stained sections of quadriceps muscle and the sections were evaluated blindly for the severity of the phenotype in each

genotype. Muscle degeneration was evaluated and scored for variation in fibre size, loss of striation, hypereosinophilia, centralised nuclei and inflammation/inflammatory cells in HE stained sections of quadriceps muscle. A severity score of 0-3 was used with 0 being unaffected, 1-weak/present, 2-medium and 3-severe.

Muscle fibrosis and calcinosis was evaluated in formalin-fixed heart tissue using van Gieson stain (Elastica van Gieson staining kit, VWR, Pennsylvania, USA) and Von Kossa stain [31] respectively. Lung pathology was evaluated and scored for alveolar oedema, congestion and alveolar histiocytosis in HE stained sections of lung tissue. A severity score of 0-3 was used with 0 being unaffected, 1-weak/present, 2-medium and 3-severe.

General locomotor activity and behavioural testing

General locomotor activity and behaviour examinations were carried out on 5-6 month old male $Stim1^{+/+}$ and $Stim1^{+/R304W}$ animals (n=10 per genotype) in an open field test, zero-maze test and endurance test in that order. To reduce bias, the experimental parameters were scored blinded to the genotypes. Mice were video-tracked during experiments (ANY-Maze™ Behavioural tracking software, Dublin, Ireland). All parameters were compared between $Stim1^{+/+}$ and $Stim1^{+/R304W}$ animals.

In the open field test, mice were introduced to a brightly lit closed maze and were monitored and video tracked for 45 minutes. The distance travelled, time spent in the centre of the maze, time spent mobile and maximum speed were monitored and automatically analysed for each mouse with the tracking system.

The endurance tests were performed in a 5-lane mouse treadmill with an electric grid (Panlab-Harvard apparatus, Barcelona, Spain). Mild electric shock of 0.2 A (adjustable 0 – 2 A) activated at 5 seconds intervals was used as motivation for mice to run. Mice were accustomed to the instrument for two days prior to test. Exercise endurance was tested by running mice till exhaustion which was defined as inability to continue running following mild electric shock, standing on electric grid for >4 seconds or running close to the grid for longer than 5 seconds. The time and distance run before reaching exhaustion were recorded.

Experiments on isolated skeletal muscle fibres

Skinned hind feet were transported overnight to the laboratory at room temperature in oxygenated 10% foetal calf serum (Gibco) supplemented DMEM media (Sigma Aldrich). The flexor digitorum brevis (FDB) muscle was split into individual digits and the central three digits were used in these experiments. Muscle fibres were isolated with a pair of micro-iris scissors and jeweler's forceps [32].

Fibres were chosen if it contracted and then relaxed upon stimulation with an electrode that delivered 1 ms, 5-8 V pulses. All other fibres were killed and removed to leave a single fibre. Platinum micro-clips were attached to the residual tendinous material and mounted in a perfusion chamber between a force transducer (AE801, Kronex Technologies, CA, USA) and an adjustable holder.

Fibres were superfused with Tyrode solution containing 121 mM NaCl, 5 mM KCl, 1.8 mM $CaCl_2$, 0.5 mM $MgCl_2$, 0.4 mM NaH_2PO_4, 24 mM $NaHCO_3$, 0.1mM EDTA, and 5.5 mM glucose at 31°C which is the temperature that the muscle fibres experience in the living foot. Solution was supplemented with 0.2% FBS and bubbled with 95% O_2 - 5% CO_2, giving a pH of 7.4. The fibre was stimulated with 15 to 150Hz, 350 ms tetani of supramaximal electrical pulses (0.5 ms in duration) delivered via platinum electrodes placed parallel to the long axis of the fibre. The length of the preparation was adjusted to the length at which tetanic force was maximal. Tetanic force was normalized to cross-sectional area and expressed as specific force (kN/m^2).

To measure resting and tetanic $[Ca^{2+}]_i$, muscle fibres were pressure injected with the fluorescent indicator Indo-1 (Molecular Probes/Invitrogen, Carlsbad, CA, USA). Indo-1 was excited at 360 ± 5 nm and the light emitted at 405 ± 5 and 495 ± 5 nm was measured with a pair of photomultiplier tubes (Photon Technology International, Wedel, Germany). Indo-1 fluorescence signals were converted into $[Ca^{2+}]_i$ as described previously [33]. Mean resting $[Ca^{2+}]_i$ was measured during the 200 ms preceding a tetanus. Tetanic $[Ca^{2+}]_i$ was measured as the mean of the final 250 ms of the 350 ms tetanus and tetanic force was measured as the peak force during the tetanus.

The force-frequency relationship was determined for each fibre by producing single tetanic contractions at different frequencies at 1 minute intervals. Fatigue was induced by stimulating fibres with a train of 150 tetani (70 Hz, 500 ms) given at 2 second intervals. Ca^{2+} entry into the fibre was assessed by a Mn^{2+}-quench method which relies on the fact that Mn^{2+} reduces the fluorescent signal of many Ca^{2+} sensitive indicators including Indo-1 and is not taken up by the SR Ca^{2+}-pumps [34]. Rested fibres were exposed to Tyrode solution containing 1 mM Mn^{2+} and the 405 nm light emission of Indo-1 was followed before, during and after exposure to Mn^{2+}.

Preparation of STIM1 R304W foetal liver cell chimeras

Foetal liver cells from E14.5 mouse embryos derived from $Stim1^{+/R304W}$ mice inter-crosses were used to generate $Stim1^{+/+}$→WT, $Stim1^{+/R304W}$→WT, and $Stim1^{R304W/R304W}$→WT chimeras as previously described [35]. The platelet specific STIM1 KO mice; *$Stim1^{fl/fl}$ PF4-Cre* have been previously described [36].

Flow cytometry studies on platelets

All flow cytometry experiments were performed using washed platelets or diluted whole blood collected into heparinised capillary tubes. Washed platelets were prepared as described previously [37]. In brief, centrifugation of diluted whole blood at 130 g for 4 minutes to obtain platelet rich plasma (PRP) followed by pelleting of platelets in the PRP in the presence of prostaglandin I2 (PGI_2, Caymen Chemical, Michigan, USA). The pellet was washed twice, and the platelets re-suspended in modified Tyrode's buffer at pH 7.4.

Platelet counting was performed in a 5 µl aliquot of heparinised whole blood labelled with the platelet specific antibody detecting GPIX (anti GPIX, clone Xia-B4, Emfret analytics) labelled with AlexaFluor-647 for 10 minutes at room temperature. The samples were diluted with 1x PBS and immediately analysed on an Accuri C6 flow cytometer (BD Bio Sciences, CA, USA). Platelets were gated on GPIX labelling and forward scatter parameters.

In order to measure platelet activation, whole blood was diluted in Tyrode's buffer containing 2 mM $CaCl_2$ (1 mM final), activated with PAR4p or Cvx for 10 minutes in the presence of antibodies recognizing activated integrin αIIbβ3 (JON/A-PE, Emfret analytics, Eibelstadt, Germany) and P-selectin expression (α-P selectin-FITC, BD Biosciences), diluted and analysed on an Accuri C6 flow cytometer. Platelets were gated on GPIX-Alexa 647 labelling and JON/A and P-selectin antibody binding was determined by mean fluorescence intensity (MFI). PS exposure was measured in washed platelets activated with PAR4p (400 µM) + Cvx (Low dose or High dose; Appropriate doses were determined by testing activation of wild-type platelets) for 10 mins in the presence of anti-GPIX-647 antibody (2 µg/ml) and AnnexinV-488 (2 µg/ml) in 1mM Ca^{2+} supplemented Tyrode buffer.

In order to measure Ca^{2+} fluxes, washed platelets were incubated with 5 µM Fluo-4-AM for 30 minutes in the absence of Ca^{2+} and then treated with 1 µM thapsigargin followed by re-introduction of 2 mM Ca^{2+}. Fluo-4 intensity was then measured over time.

For the measurement of STIM1 expression in platelets, whole blood was fixed in 4% PFA for 10 mins at RT. The cells were pelleted, and the RBCs were lysed with RBC lysis buffer for 10 min. Samples were then centrifuged and supernatant removed. The platelet/WBC pellet was washed with 1x PBS and cell counts were normalized between samples. The cells were then permeabilized with 0.5% Triton X-100 (Sigma Aldrich) for 5 mins at RT. The cell pellet obtained after centrifugation was re-suspended with PBS+1% BSA and stained with STIM1 (5ug/ml final concentration) for 10 mins at RT and co-stained with GPIX-Alexa 647 platelet marker. Secondary antibody, Alexa-488- α-rabbit was used to detect the STIM1 antibody in a 1:1000 dilution. Cells were pelleted, re-suspended in 1x PBS and analysed by flow cytometry.

Statistics

Results are presented as mean ± SEM. Chi-square test was used to calculate the statistical significance in the deviation from Mendelian birth ratio in the mouse line. Differences between $Stim1^{+/+}$ and $Stim1^{+/R304W}$ or $Stim1^{R304W/R304W}$ were assessed using Student's t-test. Graph Pad Prism 7 (GraphPad Software Inc., CA, USA) was used for statistical analyses and graph plots.

Statistical analyses of $[Ca]_i$ were performed using the SigmaPlot software (Systat Software, Inc., San Jose, CA, USA). Unpaired or paired t-tests were applied to compare the differences between groups. A p-value <0.05 was defined as statistically significant.

Results

Generation of the $Stim1^{R304W}$ mouse model

A knock-in mouse line expressing the *Stim1* (NC_000073.6) chr7:102421471A>T (GRCm38.p4) mutation was established using the CompoZr™ ZFN technology [38]. Out of 144 progeny, two heterozygous $Stim1^{+/R304W}$ founder females were identified. Targeted insertion of the *Stim1* mutation was confirmed in the two founders by Sanger sequencing of a PCR fragment obtained with primers flanking the region corresponding to the ZNF modification template (chr7:102420366-102422512 bp, GRCm38/mm10). One founder died spontaneously before breeding, and thus the line described here originated from a single female founder mouse. Whole genome sequencing of DNA from the founder mouse detected no off-target insertions of the repair template in the genome and confirmed the specific *Stim1* chr:7102421471A>T substitution with no other modifications in *Stim1*. Thus, the mouse line generated carried a mutation that resulted in the R304W substitution in STIM1, and is hereafter referred to as $Stim1^{R304W}$.

Lethality of the $Stim1^{R304W/R304W}$ mice

Crossbreeding of heterozygous animals was performed to generate homozygous mice. Following 25 heterozygous crosses, 130 offspring survived more than three days. The total number of pups obtained and the genotype ratio in these mice, 36:91:3 ($Stim1^{+/+}$:$Stim1^{+/R304W}$:$Stim1^{R304W/R304W}$), deviated significantly from the expected Mendelian ratio (chi-square test: p<0.0001) (Supplementary Table 3), highlighting the lethality of the $Stim1^{R304W/R304W}$ mice.

Examination of embryos following 14 $Stim1^{+/R304W}$ x $Stim1^{+/R304W}$ timed crosses revealed litter sizes ranging from 2 to 11 embryos (average 6.6), with less than 10 residual bodies or resorption sites observed in total. The genotype ratio in embryos extracted at 12.5, 13.5, 14.5, 15.5, 16.5 and 17 dpc

was 20:53:19 ($Stim1^{+/+}$:$Stim1^{+/R304W}$:$Stim1^{R304W/R304W}$), which did not deviate from the Mendelian ratio (Supplementary Table 4). The pups found dead or euthanized at P_0-P_1 stages showed a genotype ratio of 14:27:25 ($Stim1^{+/+}$:$Stim1^{+/R304W}$:$Stim1^{R304W/R304W}$), demonstrating no decrease in the fraction of $Stim1^{R304W/R304W}$ pups at parturition. Taken together these data show survival of $Stim1^{R304W/R304W}$ embryos up to late gestational stages with subsequent perinatal lethality.

On inspection, the $Stim1^{R304W/R304W}$ embryos appeared slightly smaller than their littermates, without apparent dysmorphisms (Figure 1A). As cyanosis was not observed in the dead P_0-P_1 pups, respiratory distress or defects in blood oxygenation were considered unlikely causes of death. Histological examinations of the diaphragm performed in formalin-fixed, paraffin-embedded sections from three 14.5 dpc $Stim1^{R304W/R304W}$ embryos revealed no obvious abnormalities in morphology or thickness of the diaphragms (Figure 1B).

Guided by the thrombocytopenia and bleeding diathesis in patients with Stormorken syndrome expressing the STIM1 R304W GoF mutation and by the lethal bleeding disorder observed in *$Stim1^{Sax}$* GoF mouse model [9, 17], embryos were examined macroscopically for signs of bleeding and blood and lymphatic vascular mixing. No visible signs of bleeding or differences in the fraction of platelets were detected in blood from $Stim1^{R304W/R304W}$ embryos at 15-17 dpc compared to their $Stim1^{+/R304W}$ and $Stim1^{+/+}$ littermates (Figure 1A and C). Thus, bleeding and thrombocytopenia were unlikely to underlie the lethality documented in the homozygous $Stim1^{R304W}$ mice.

The mutant allele is expressed in the $Stim1^{R304W}$ mice

To verify the expression of the *Stim1* mutant allele, immunohistochemistry (IHC) staining was performed on skin sections from homozygous mice. Specific STIM1 staining was detected in $Stim1^{+/+}$ and $Stim1^{R304W/R304W}$ mice (Figure 2A, left and center), but not in cells from an epithelial cell specific Stim1/Stim2 double KO mouse (DKO) [39], which served as a negative control (Figure 2A, right). Furthermore, STIM1 expression was detected by immunofluorescence (IF) microscopy in tissues of endodermal, mesodermal, and ectodermal origin including skeletal muscle, heart, lungs and choroid plexus in the $Stim1^{R304W/R304W}$ mice (Figure 2B).

Constitutive STIM1 activation in $Stim1^{R304W}$ mice

To explore the functional effect of the mutation in the $Stim1^{R304W}$ mice, we performed whole cell Ca^{2+} flux measurements in cultured skin-derived fibroblasts from P_0-P_2 day old mice. Representative traces are illustrated in Figure 3A (top panels). At baseline, intracellular cytosolic Ca^{2+} levels ($[Ca^{2+}]_i$) were significantly lower in fibroblasts from $Stim1^{+/R304W}$ mice than in wildtype mice ($p<0.02$), and also tended to be lower in $Stim1^{R304W/R304W}$ fibroblasts (Figure 3A, lower-left panel). SOCE was assessed by depleting Ca^{2+} stores with thapsigargin in Ca^{2+}-free conditions, followed by subsequent

reintroduction of Ca^{2+}. Similar magnitude SOCE was observed in wildtype, $Stim1^{+/R304W}$ and $Stim1^{R304W/R304W}$ cells (Figure 3A, lower-right panel). In contrast, skin-derived fibroblasts from patients carrying the same mutation showed significantly elevated resting $[Ca^{2+}]_i$ under basal conditions ($p<0.02$) and increased SOCE compared to healthy controls ($p<0.05$) (Figure 3B).

Measurements of STIM1 protein levels in homozygous skin-derived fibroblasts showed an approximate 3-fold reduction in STIM1 expression in $Stim1^{R304W/R304W}$ mice compared to $Stim1^{+/+}$ littermates ($p<0.05$) (Figure 3C), while STIM1 protein level was comparable in fibroblasts from patients and controls (Figure 3D). Thus, in the fibroblasts from patients, the expression of the constitutively active R304W mutation in STIM1 at normal protein levels resulted in increased resting $[Ca^{2+}]_i$, and SOCE. In contrast, over-activity of STIM1 was counterbalanced in $Stim1^{R304W/R304W}$ mice by reduced protein expression.

To further characterise the effect of the *Stim1* R304W mutation in murine cells, YFP tagged mouse STIM1-WT and mouse STIM1-R304W expression vectors were co-transfected with untagged wildtype mouse *Orai1* expression vector into NIH 3T3 cells. Greater aggregation of the YFP-signal was detected under resting conditions in cells transfected with the STIM1-R304W-YFP vector than in those transfected with STIM1-WT-YFP (Figure 3E). This was manifested as distinct fluorescent puncta, found at lower density than in those in WT-transfected cells ($p<0.05$), with increased fluorescence intensity ($p<0.02$) (Figure 3E graphs). These findings show that the R304W mutation results in constitutive STIM1 activation and oligomerization.

$Stim1^{R304W/R304W}$ mice show reduced muscle mass and reduced endurance

Three homozygous $Stim1^{R304W}$ female animals survived until they were euthanized and necropsied at 5-6 months of age. They showed reduced body size (Figure 4A) and significantly reduced body weight compared to $Stim1^{+/+}$ and $Stim1^{+/R304W}$ littermates ($p<0.05$ at 10 weeks age and $p<0.0001$ at 20 weeks age) (Figure 4B). They also exhibited reduced hind limb muscle mass and a near absence of pectoral muscles in comparison with their $Stim1^{+/+}$ and $Stim1^{+/R304W}$ littermates (Figure 4C).

There were no significant differences in general locomotor activity such as distance travelled, average speed, maximum speed and total time mobile in an open-field test in the $Stim1^{+/R304W}$ compared to $Stim1^{+/+}$ mice (n=10 per genotype, data not shown). However, in endurance examination, performance was severely reduced in the three surviving $Stim1^{R304W/R304W}$ mice compared to $Stim1^{+/R304W}$ and wildtype mice ($p<0.002$, Figure 4D).

$Stim1^{R304W}$ mice show skeletal muscle degeneration

Histological evaluation was performed in order to assess if heart or lung pathology may play a role in the reduced endurance observed in the $Stim1^{R304W/R304W}$ mice. No connective tissue ingrowth or Ca^{2+}

salt deposits were detected by van Gieson stain and Von Kossa stain in the ventricular walls or in the atrium. Hematoxylin and eosin (HE) staining of the lung sections in the homozygous Stim1^{R304W} mice showed no alveolar oedema, congestion or alveolar histiocytes, indicating an absence of cardiac pulmonary pathologies (data not shown). These results suggest that the reduced endurance is not related to heart and lung defects in these animals.

HE staining of quadriceps muscles from 5-6 months old animals showed muscle degeneration in Stim1$^{+/R304W}$ mice of both genders and in the three surviving Stim1$^{R304W/R304W}$ mice. Staining in quadriceps muscle cross sections in Stim1$^{R304W/R304W}$ mice showed marked variation in fibre size and infiltration of mononuclear cells indicating inflammation compared to wildtype mice (Figure 5A-B, top). The number of muscle fibres with centralised nuclei were increased in the Stim1$^{+/R304W}$ (data not shown) and Stim1$^{R304W/R304W}$ mice compared to wildtypes (Figure 5B, top), indicating both muscle degeneration and regeneration. Longitudinal sections of muscles from Stim1$^{R304W/R304W}$ mice showed an increased number of hypereosinophilic cells and loss of the characteristic striation pattern (Figure 5B, bottom). Blinded severity scoring of muscle fibre size, loss of striation, hypereosinophilia, centralised nuclei, and inflammation showed a significantly increased severity score of degeneration in Stim1$^{R304W/R304W}$ ($p<0.0001$) mice compared to the wildtype mice (Figure 5C). Severity scoring in quadriceps from Stim1$^{+/R304W}$ mice also showed a significantly increased mean score ($p<0.05$) compared to the wildtypes. No signs of muscle degeneration were observed in the age-matched Stim1$^{+/+}$ animals. HE stains of diaphragm in adult Stim1$^{+/R304W}$ showed a slight increase in the mean score of degeneration of the diaphragm compared to Stim1$^{+/+}$. However, the scoring showed a variation between the heterozygous animals, while the one Stim1$^{R304W/R304W}$ diaphragm analysed showed an elevated score (Supplementary Figure 1).

STIM1 expression was detected in skeletal muscle in the wildtype and most fibres from three surviving Stim1$^{R304W/R304W}$ mice on IHC stained sections of the quadriceps (Figure 5D-E). However, the STIM1 level was too low to be detected on western blots indicating a marked reduction in STIM1 expression relative to wildtype (Figure 5F).

Cellular muscle function was studied in intact single flexor digitorum brevis (FDB) fibres of adult Stim1$^{+/R304W}$ and Stim1$^{+/+}$ mice [32]. Resting $[Ca^{2+}]_i$ did not differ between Stim1$^{+/+}$ and Stim1$^{+/R304W}$ fibres. The $[Ca^{2+}]_i$-frequency and force-frequency relationships were studied by stimulating fibres with brief (350 ms) trains of electrical pulses at 1 minute intervals. Tetanic $[Ca^{2+}]_i$ and force were similar in Stim1$^{+/R304W}$ and Stim1$^{+/+}$ fibres, and the $[Ca^{2+}]_i$-frequency and force-frequency relationships were virtually identical in the two groups (Figure 6A-B). Average $[Ca^{2+}]_i$ and force records from 70 Hz tetanic stimulations show clearly that there were no differences in the time course of changes in $[Ca^{2+}]_i$ and force at the onset of contraction or during the relaxation after the end of stimulation

(Figure 6C-D). As a result of fatigue induced by 150 repeated 70 Hz tetanic contractions, resting $[Ca^{2+}]_i$ increased and tetanic $[Ca^{2+}]_i$ and force decreased to a similar degree in $Stim1^{+/R304W}$ and $Stim1^{+/+}$ FDB fibres (Figure 6E-G).

Mn^{2+} ions traverse most Ca^{2+} permeable channels and can substitute for Ca^{2+} in SOCE but are not taken up by the SR Ca^{2+}-pumps. Once inside the cell, Mn^{2+} quenches the fluorescence signal of fluorescent indicators, including Indo-1. Figure 6H shows the general procedure for carrying out the Mn^{2+} quench experiments and the mean data in Figure 6I show that the influx of Mn^{2+} was not significantly different in $Stim1^{+/+}$ and $Stim1^{+/R304W}$ fibres. Together these results indicate no differences in $[Ca^{2+}]_i$ handling and force production in isolated muscle fibres between $Stim1^{+/R304W}$ and wildtype mice.

Platelets from $Stim1^{R304W/R304W}$ mice showed normal numbers, but lacked STIM1 expression

In the $Stim1^{+/R304W}$ mice and in two surviving $Stim1^{R304W/R304W}$ mice, red and white blood cell counts (total and differential), haemoglobin levels, mean cell volume, haematocrit and calculated free serum Ca^{2+} levels showed counts within reference ranges and comparable to $Stim1^{+/+}$ animals (data not shown). In addition, flow cytometry on blood samples from $Stim1^{+/R304W}$ mice showed normal platelet numbers (Figure 7A) and size (data not shown).

Due to the lethality of $Stim1^{R304W/R304W}$ mice, the consequences of the R304W mutation in the haematological lineage were studied in foetal liver cell chimeric mice. Three $Stim1^{R304W/R304W}$→WT, two $Stim1^{+/R304W}$→WT and four $Stim1^{+/+}$→WT chimeras were created. Following a 4-6 week recovery period post transplantation, Sanger sequencing detected DNA only from the donor cells in peripheral blood samples from the chimeric mice, documenting an efficient reconstitution of the haematopoietic cell lineage in these animals (Supplementary Figure 2). Platelet counts of $Stim1^{+/R304W}$→WT and $Stim1^{R304W/R304W}$→WT chimeric animals were within reference ranges and comparable to $Stim1^{+/+}$→WT controls (Figure 7B). Intracellular staining demonstrated significantly reduced expression of STIM1 protein in platelets isolated from $Stim1^{+/R304W}$→WT and $Stim1^{R304W/R304W}$→WT chimeric animals when compared to controls (Figure 7C). In fact, STIM1 staining in $Stim1^{R304W/R304W}$→WT platelets was as low as that in platelets isolated from platelet specific *Stim1* knockout mice. In contrast, STIM1 protein expression was detectable in leukocytes from $Stim1^{R304W/R304W}$→WT chimeras (Figure 7D). Absence of STIM1 expression was confirmed in platelets and megakaryocytes from $Stim1^{R304W/R304W}$→WT chimeras by western blotting (Figure 7E) and in fetal liver in Stim1R304W/R304W embryos by immunofluorescence staining (Figure 7F). Quantification of the transcript level by real-time quantitative PCR (qPCR) of cDNA derived from whole blood RNA demonstrated a significant reduction in the Stim1 levels in $Stim1^{+/R304W}$ mice

compared to wildtype mice ($p<0.05$) (Supplementary Figure 3). In platelets from patients with Stormorken syndrome expressing the STIM1 R304W mutation and healthy controls, however, similar STIM1 expression was observed by western blot (Figure 7E, bottom). Together these results indicate a significant reduction of STIM1 expression in the megakaryocytic lineage of the STIM1 R304W mutant mice, which differs from the patients with Stormorken syndrome.

No SOCE and impaired activation of homozygous Stim1 ^{R304W} platelets

In line with reduced STIM1 expression, platelets from Stim1$^{+/R304W}$→WT mice showed slightly reduced SOCE following Ca^{2+} depletion with thapsigargin, while no SOCE induction was detected in platelets from Stim1$^{R304W/R304W}$→WT chimeras (Figure 8A). Platelets from Stim1$^{+/R304W}$→WT chimeras showed markedly reduced Ca^{2+} induced Ca^{2+} entry compared to Stim1$^{+/+}$ and platelets from Stim1$^{R304W/R304W}$→WT chimeras completely lacked Ca^{2+} influx following re-introduction of Ca^{2+} in extracellular media (Figure 8B).

Platelet activation studies were performed on Stim1$^{R304W/R304W}$→WT and Stim1$^{+/R304W}$→WT chimeric mice using the immunoreceptor tyrosine-based activation motif (ITAM) receptor agonist, convulxin, (Cvx) and the G-protein coupled receptor (GPCR) agonist, Par4 activating peptide (Par4p). Platelets from Stim1$^{R304W/R304W}$→WT mice and mice lacking STIM1 in the megakaryocyte lineage (KO) showed impaired activation of integrin αIIbβ3 (Figure 8C) and impaired granule secretion (Figure 8D) in response to low dose (LD) and high dose (HD) Cvx. Similar results were obtained with platelets activated with PAR4p (data not shown). Stim1$^{+/R304W}$→WT platelets showed a normal integrin activation and granule secretion response. We previously demonstrated that SOCE is particularly important for the platelet pro-coagulant response, i.e. their ability to externalize phosphatidylserine (PS) and to assemble plasma clotting factors on their cell surface [36]. Consistent with the reduced STIM1 protein levels, platelets from both Stim1$^{+/R304W}$→WT and Stim1$^{R304W/R304W}$→WT chimeras showed a significant defect in AnnexinV binding (a measure of surface PS exposure) in response to stimulation with Par4p and Cvx agonists (Figure 8E).

Discussion

We generated a mouse line expressing the STIM1 R304W mutant protein. The specific integration of the mutation was verified by on-target PCR and by whole genome sequencing of the founder mouse. The mutant protein showed expression in most tissues assessed in heterozygous and homozygous embryos and adult mice. However, we detected a reduced level of STIM1 in homozygous $Stim1^{R304W/R304W}$ haematopoietic cells, fibroblasts and skeletal muscle, which appears to effectively compensate for constitutive activity of the protein.

Although *STIM1* GoF mutations are pathogenic in humans and mice, our results contribute to a growing consensus that the specific consequences of these mutations may be species dependent. The *Stim1* EF-hand GoF, D84G, mutation caused a severe bleeding disorder resulting in embryonic lethality in the $Stim1^{Sax}$ mice [17], but it causes only TAM in humans [8]. In humans, the R304W mutation results in constitutively active STIM1 causing Stormorken syndrome, a multi-organ disease which includes TAM [9, 12, 18-19]. The results presented here suggest that the *Stim1* R304W encodes a constitutively active protein also in mice, with the protein being expressed at reduced levels in skin fibroblasts, skeletal muscle and in haematopoietic cells. The reduced expression of a constitutively active STIM1 R304W protein explains the similar resting $[Ca^{2+}]_i$ and SOCE amplitude detected in the fibroblasts from $Stim1^{+/+}$ and $Stim1^{R304W/R304W}$ mice, despite the 3 fold reduction in STIM1 levels in the latter.

All but three homozygous $Stim1^{R304W}$ mice died perinatally. The requirement of a well-regulated SOCE during embryonic and neonatal stages is demonstrated by the lethality of the *Stim1* KO mouse models [40-41]. Both the $Stim1^{R304W}$ and the $Stim1^{Sax}$ GoF mouse models with constitutive STIM1 activation manifested homozygous lethality [17], but stage and aetiology of the lethality were profoundly different. The homozygous $Stim1^{R304W}$ embryos did not show the bleeding and the blood lymphatic vascular mixing seen in $Stim1^{Sax}$ mice which caused death as early as <14.5 dpc [17]. Conceivably the lack of STIM1 in platelets and megakaryocytes explains the lack of bleeding in the $Stim1^{R304W}$ embryos and survival until birth. Platelet specific *Stim1* KO was not lethal in mice [36], therefore the perinatal lethality in the homozygous $Stim1^{R304W}$ mice was likely not caused by the lack of STIM1 in platelets. Common causes of perinatal lethality involve problems at parturition, such as abnormalities in breathing, suckling and homeostasis [42]. However, we detected no cyanosis or morphological abnormalities in the diaphragm in the homozygous $Stim1^{R304W}$ pups that were found dead at day P0, which would have indicated breathing dysfunction. Lethality of the global *Stim1* KO was ascribed to dysfunction in respiratory muscle [41]. However, lethality was also observed in skeletal muscle specific *Stim1* KO and smooth muscle specific *Stim1* KO mice, highlighting the importance of STIM1-mediated SOCE in both types of muscle at early developmental stages [40, 43].

A large body of evidence underscores the importance of STIM1 and ORAI1 mediated regulation of Ca^{2+} signalling during skeletal muscle development (reviewed in [44] [45]). The STIM1 expression is developmentally regulated and it peaks postnatally in skeletal muscle in mice [46]. Furthermore, patients that lack SOCE due to *STIM1* mutations present with congenital skeletal muscle myopathy [11, 47] and mice lacking functional STIM1 in skeletal muscles died in perinatal stages from a skeletal muscle myopathy [14, 43]. Growth, differentiation and regeneration of muscle after birth are also dependent on STIM1 regulated Ca^{2+} signalling; for instance, a skeletal-muscle-specific STIM1 transgenic mouse model showed signs of muscle degeneration (35). In contrast, humans with GoF *STIM1* mutations manifest myopathy and TAM, but no muscle degeneration [6, 9, 16]. No muscular phenotype was reported in heterozygous GoF $Stim1^{Sax}$ mice [17]. We presently show markedly decreased muscle mass and reduced endurance exercise performance in the three surviving $Stim1^{R304W/R304W}$ mice, and our histological investigation of the skeletal muscle showed muscle degeneration and regeneration. On the other hand, we did not detect any significant differences between $Stim1^{+/R304W}$ and wildtype mice regarding either *in vivo* endurance exercise performance or $[Ca^{2+}]_i$ handling and force production in isolated muscle fibres in the rested state or during fatigue.
Major changes in STIM1 function are accompanied by marked alterations in skeletal muscle, or even an absence of skeletal muscle phenotype. Conversely, contractile activity, including fatiguing exercise, in adult skeletal muscle fibres mainly depends on bi-directional Ca^{2+} fluxes between the sarcoplasmic reticulum and the cytosol. SOCE may therefore be of limited importance for contractile function in the short-term [48], which can explain the apparently functional skeletal muscles in $Stim1^{+/R304W}$ mice. However, further studies are required to reveal the exact mechanisms involved in the role of SOCE in long-term muscle maintenance at adult stages.

Previous work showed elevated resting $[Ca^{2+}]_i$, constitutive SOCE and impaired platelet function leading to a bleeding diathesis in patients with Stormorken syndrome, as well as variable severity of thrombocytopenia [9, 12]. Impaired platelet activation and function in *Stim1*^{Sax} and *Stim1* KO mice, also highlight the importance of STIM1 for platelet functions [17, 41]. Furthermore, *Stim1* GoF mutations resulted in embryonal lethality due to bleeding in the $Stim1^{Sax}$ mice [17]. When we assessed the STIM1 expression in a range of tissues in the $Stim1^{R304W}$ mice and in chimeric mice, we detected reduced expression in platelets, megakaryocytes and leucocytes. Interestingly, the data indicated that the level of the *Stim1* mutant transcript was reduced compared to the wildtype transcript which resulted in reduced protein levels in heterozygotes and especially in homozygotes compared to cells from the wildtype mice. In fact, no STIM1 protein expression was detected in megakaryocytes and platelets in $Stim1^{R304W/R304W}$ mice and $Stim1^{R304W/R304W}$→WT chimeras, resulting

in a platelet specific STIM1 KO. In line with the observations previously described in the platelet specific *Stim1* KO mice [36], the homozygous Stim1^{R304W} mice and the chimeras with undetectable STIM1 levels, showed impaired platelet activation, no SOCE and presented with normal platelet counts.

Conclusion

We describe a *Stim1* knock-in mouse model expressing the constitutive STIM1 R304W mutation. The perinatal lethality and the severe muscle degeneration documented in the Stim1^{R304W} line highlight the critical role of a tightly controlled SOCE for skeletal muscle development and long-term integrity. We showed a specific reduction of the mutant protein in particular in the haematopoietic lineage, where it possibly compensated constitutive STIM1 activation and prevented cytosolic Ca^{2+} overload. Understanding what promotes downregulation of STIM1 in this mouse model but not in the patients with Stormorken syndrome carrying the same R304W mutation is the obvious next step to study.

Competing Interests

There are no conflicts of interests to declare.

Acknowledgements

We are grateful to the patients who participated in this study and provided biological samples. We thank Ms. Guro Lien, Ms. Turid Pedersen from Oslo University Hospital, Oslo, for their valuable input to the project, technical assistance in embryo's extractions, and flowcytometry studies, respectively. Histological services for embryo characterization were provided by the Histology Research Core Facility at the Department of Cell Biology and Physiology, University of North Carolina, Chapel Hill NC. We also thank Ms. Claire Trincot at Kathleen Caron lab, University of North Carolina, Chapel Hill NC for their assistance and input in immune fluorescence based staining of mouse embryo sections. T.G was supported financially by the Quota scheme of Norwegian State Educational Loan Fund, "Mobility grant for PhD students by the Institute for Clinical medicine, University of Oslo and by UNIFOR. W.B was supported through a grant from National Institute of Health, USA (R01 HL130404), and R.H.L was funded by T32 HL007149. H.W was supported by the Swedish Research Council (K2014-52X-10842-21-5).

Figure legends

Figure 1. Evaluation of Stim1^{R304W} embryos.

(A) Representative images of embryos at 15.5 dpc showed overall normal morphology and development with slightly smaller body size in Stim1$^{R304W/R304W}$ embryos (Hom) compared to heterozygous Stim1$^{+/R304W}$ (Het) and Stim1$^{+/+}$ (WT) littermates. Scale bar= 5mm.

(B) No apparent abnormalities in morphology were detected in the HE stained sections of paraffin embedded embryos at 16.5 dpc. The diaphragms (indicated by black boxes) of the analysed sections showed no signs of abnormal thickness or degeneration (bottom).

(C) Whole blood from embryos at E15-E18 stages showed similar fraction of platelets in WT (n=4), Het (n=20) and Hom (n=9) mice. The platelet fractions were measured by flow cytometry as the percentage of cells positive for the platelet marker GPIX.

Figure 2. *Stim1* expression in tissues from Stim1^{R304W} mice.

(A) STIM1 IHC in adult paw skin demonstrates strong cytoplasmic STIM1 staining (brown) in epidermal keratinocytes in Stim1$^{+/+}$ (WT, left), and Stim1$^{R304W/R304W}$ mice (Hom, middle). No staining was detected in the epithelial cell specific *Stim1/2* double KO mouse (DKO, right) [39].

(B) STIM1 immunofluorescence (IF) in whole mount homozygous Stim1^{R304W} embryos at 16.5 dpc demonstrates STIM1 staining (green) in cells of mesodermal origin (skeletal muscle cells and cardiac muscle cells), in cells of endodermal origin (lung cells), and in cells of ectodermal origin (cells in choroid plexus), as indicated.

Figure 3. Calcium handling in human and neonatal mouse fibroblast cells.

(A) Whole cell Ca^{2+} measurements were performed in cultured skin-derived fibroblast cells from neonatal mice. Representative recordings and mean data (top and lower panels, respectively) show that under baseline conditions, resting $[Ca^{2+}]_i$ was significantly lower in fibroblasts from heterozygous Stim1$^{+/R304W}$ mice (Het, n=93 cells) compared to wildtype Stim1$^{+/+}$ (WT, n=76 cells, $p<0.02$), and tended to be lower in homozygous Stim1$^{R304W/R304W}$ (Hom, n=95 cells). Following Ca^{2+} store depletion with 2 μM thapsigargin and Ca^{2+}-free conditions, reintroduction of 10 mM Ca^{2+} revealed similar magnitude SOCE in WT, Het, and Hom cells (n=66, 86, 78 cells, respectively).

(B) A similar experiment performed in human fibroblast cells showed significantly elevated resting Ca^{2+} levels in cells from patients with Stormorken syndrome (n=39 cells) compared to healthy controls (n=39 cells) ($p<0.02$). Fibroblasts from the two patients (n=26 cells) also exhibited augmented SOCE compared to control cells (n=14 cells) ($p<0.05$).

(C) Western blot results showed significant reduction of STIM1 expression in fibroblasts from homozygous animals (Hom) compared to Stim1$^{+/+}$ (WT) ($p<0.05$); β-actin was used as a loading control.

(D) No difference in STIM1 expression was detected in fibroblast cells of two patients with Stormorken syndrome [9] compared to healthy controls, as indicated.

(E) Representative images of NIH 3T3 murine cells transfected with mouse STIM1-WT-YFP or STIM1-R304W-YFP plasmids. Cells transfected with mouse STIM1-R304W-YFP showed increased clustering of YFP signal at resting conditions indicating constitutive STIM1 aggregation and activation (left). Measurement of fluorescence intensity of STIM1-YFP signal in regions of interest (red outlines in lower panel) in STIM1-R304W-YFP (n=12) transfected cells showed a 28% decrease in aggregate density ($p<0.05$) compared to STIM1-WT-YFP (n=10) and a 63% increase in mean intensity ($p<0.02$) (right).

In all panels, p-values for significance are indicated as: ns=not significant, *=$p<0.05$, **=$p<0.02$, ****=$p<0.0001$.

Figure 4. Reduced growth and endurance in Stim1^{R304W} mice.

(A) Homozygous Stim1$^{R304W/R304W}$ (Hom) mice showed reduced overall body size compared to their heterozygous Stim1$^{+/R304W}$ (Het) and wild type Stim1$^{+/+}$ (WT) littermates. Mice were 5 months old at the time of imaging. Scale bar= 1 cm.

(B) Female wildtype and heterozygous mice followed similar growth curves, while female homozygous mice showed reduced linear growth. Each curve represents an average weight of ≥3 animals with significant differences at age 10 weeks ($p<0.05$) and 20 weeks ($p<0.0001$) between wildtype and homozygous mice.

(C) Homozygous Stim1$^{R304W/R304W}$ (Hom) mice showed reduced pectoral muscle mass and hindlimb muscle mass (arrow, bottom) compared to their heterozygous littermates (Het).

(D) Test of endurance in wildtype, heterozygous and homozygous mice measured with distance run on treadmill showed significantly reduced endurance in homozygous mice (Hom, n=3) compared to age matched wildtype mice (WT, n=21) ($p<0.005$). Endurance in heterozygous mice (Het, n=21) was similar to the wildtype controls.

In all panels, p-values for significance are indicated as: ns=not significant, *=$p<0.05$, ***=$p<0.005$, ****=$p<0.0001$.

Figure 5. Skeletal muscle degeneration in Stim1^{R304W} mice

(A) Cross-section (top) and longitudinal section (bottom) of HE stained quadriceps muscles showed regular fibre structure and diameter and peripheral nuclei with presence of characteristic striation in Stim1$^{+/+}$ wildtype mice (WT).

(B) Stim1$^{R304W/R304W}$ homozygous (Hom) mice showed basophilic fibres containing centralized nuclei (top, arrowheads), irregular fibre diameter and staining intensity (top, arrow), aggregates of inflammatory cells (bottom, arrowhead) and degenerated muscle fibres (bottom, arrow).

(C) Severity scoring of skeletal muscle degeneration parameters of mice with all three genotypes. Quadriceps muscle showed significant degeneration in Stim1$^{+/R304W}$ heterozygous (Het, n=18) ($p<0.05$) and homozygous (Hom, n=3) ($p<0.0001$) compared to wildtypes (WT, n=7). Sections were scored for degeneration on variation in fibre size, loss of striation, hypereosinophilia, centralised nuclei and inflammation/inflammatory cells with a score of 0-3 (0-unaffected, 1-weak/present, 2-medium and 3-severe) with a potential maximum total score of 15.

(D) IHC show homogenous STIM1 staining in quadriceps muscle fibres from $Stim1^{+/+}$ mice.

(E) Some STIM1 staining was detected (arrow) but most was lost in degenerate fibres in quadriceps from homozygous mice (arrowhead).

(F) Western blot on proteins extracted from frozen skeletal muscle samples shows STIM1 expression in lysates from $Stim1^{+/+}$ (WT) but not in lysates from homozygous animals (Hom); GAPDH was used as a loading control.

p-values for significance are indicated as: *=p<0.05, ****=p<0.0001.

Figure 6. Ca^{2+} handling in mouse FDB fibres.

(A-B) Tetanic $[Ca^{2+}]_i$-frequency (A) and force-frequency relationships (B) in FDB fibres from wildtype (WT, n=9 fibres) and heterozygous $Stim1^{+/R304W}$ (Het, n=7 fibres) mice showed no difference between the two groups. Tetani were evoked at 1 minute intervals.

(C-D) Comparable averaged tetanic $[Ca^{2+}]_i$ records (C) and force records (D) were observed from 70 Hz tetanic contractions in wildtype (WT, n=9) and $Stim1^{+/R304W}$ heterozygous (Het, n=7) FDB fibres from at least three mice in each group.

(E-G) Resting $[Ca^{2+}]_i$ (E), tetanic $[Ca^{2+}]_i$ (F), and tetanic force (G) were similar in wildtype (n=6) and $Stim1^{+/R304W}$ (n=5) FDB fibres both at the start and end of fatigue induced by 150 repeated tetani. Symbols represent the individual values obtained in fibres.

(H) A typical record of the Indo-1 fluorescent signal at 405 nm during a Mn^{2+} quenching experiment performed to assess SOCE in a single FDB fibre. Mn^{2+} present during the experiment indicated.

(I) Mn^{2+} quenched the Indo-1 signal at the same rate in wildtype (WT, n=5) and heterozygous $Stim1^{+/R304W}$ (Het, n=11) fibres.

Figure 7. Platelet counts and STIM1 expression in $Stim1^{R304W}$ mice.

(A) Platelet counts in adult wildtype $Stim1^{+/+}$ (WT, n=8) and heterozygous $Stim1^{+/R304W}$ (Het, n=12) mice were within reference ranges (reference mean platelet count= 1-1.3x10^9/ml).

(B) Foetal liver cell chimeric mice from all three *Stim1* genotypes showed platelet counts within reference ranges (reference mean platelet count= 1-1. 3x10^9/ml, WT: n=4, Het: n=2, Hom: n=3).

(C-D) STIM1 expression in platelets (P) and leucocytes (L) measured by flow cytometry in chimeric mice. (C) In platelets, the expression was significantly reduced in heterozygous $Stim1^{+/R304W}$ →WT (Het, n=6) (p<0.0001) and homozygous $Stim1^{R304W/R304W}$→WT mice (Hom, n=3) (p<0.0001) compared to WT (n=5). (D) Similarly, in leucocytes the STIM1 expression was significantly reduced in homozygous $Stim1^{R304W/R304W}$→WT mice (n=3) (p<0.05), but not in platelet-specific *Stim1* knockout mice (KO).

(E) Western blot analysis documents reduced STIM1 expression in platelets from $Stim1^{R304W}$ mice (top) while platelets from two patients with Stormorken syndrome (P1 and P2) show similar levels compared to healthy controls (C1-4) (bottom). Expression of β-actin was used as a loading control.

(F) Immunofluorescence staining of STIM1 in 14.5 dpc embryonic liver from wildtype (WT), heterozygous (Het) and homozygous $Stim1^{R304W}$ (Hom) embryos detected STIM1 expression in WT and heterozygous, but not in homozygous megakaryocytes (arrowheads).

In panels C and D, p-values for significance are indicated as: *=p<0.05, **=p<0.02, ****=p<0.0001.

Figure 8. SOCE and platelet activation assessed in $Stim1^{R304W}$ chimeric mice by flow cytometry.

(A) Platelets from chimeric mice were washed and loaded with Fluo-4-AM, and Fluo-4 intensity was measured in real time by flow cytometry. Store operated Ca^{2+} entry (SOCE) in platelets was assessed by incubation with thapsigargin in Ca^{2+}-free buffer, followed by the reintroduction of 2 mM Ca^{2+}. Homozygous $Stim1^{R304W/R304W}$→WT platelets (Hom→WT) did not show thapsigargin induced SOCE, which was detected in heterozygous $Stim1^{+/R304W}$→WT (Het→WT) and WT (WT→ WT) platelets.

(B) Heterozygous $Stim1^{+/R304W}$→WT platelets showed reduced Ca^{2+} induced Ca^{2+} entry compared to WT (WT→ WT) platelets, while homozygous $Stim1^{R304W/R304W}$→WT (Hom→WT) platelets showed lack of Ca^{2+} induced Ca^{2+} entry.

(C-D) Platelets stimulated with low doses (LD) and high doses (HD) of Cvx showed impaired activation of homozygous platelets measured by Integrin activation with JON/A-PE antibody (C) and reduced granule secretion with anti-P-selectin antibody (D). Significantly impaired activation was detected at both LD (p<0.05) and HD (p<0.02) Cvx in homozygous platelets. (WT→ WT: n=6, Het→WT: n=4, Hom→WT: n=5)

(E) Dual agonist stimulation (Par4p + Cvx) in washed platelets to induce phosphatidylserine (PS) exposure showed significant impairment of PS exposure measured with AnnexinV-488 in heterozygous (Het→WT, n=2) (p<0.05) and homozygous (Hom→WT, n=3) (p<0.0001) compared to WT (WT→WT, n=2) platelets.

In panels C, D and E, p-values for significance are indicated as: *=p<0.05, **=p<0.02, ***=p<0.005.

Supplementary material

Supplementary Table 1. List of primers.

Supplementary Table 2. List of antibodies.

Supplementary Table 3. Chi-square test showed a significant deviation from the expected Mendelian ratio in live animals after 25 $Stim1^{+/R304W}$ X $Stim1^{+/R304W}$ crosses ($p<0.0001$).

Supplementary Table 4. Chi-square test showed no statistically significant deviation from the expected Mendelian ratio in embryos observed *in utero* after 14 $Stim1^{+/R304W}$ X $Stim1^{+/R304W}$ crosses.

Supplementary Figure 1. Severity scoring of muscle degeneration parameters in HE stained sections of diaphragm muscle of 20±2 weeks old mice show no significant degeneration in $Stim1^{+/R304W}$ heterozygous (Het, n=15) muscle compared to wildtypes (WT, n=4). The means score of degeneration in heterozygous diaphragm muscle show a slight increase in degeneration with a variation between animals. $Stim1^{R304W/R304W}$ homozygous (Hom) (n=1) showed a total score of 10 in degeneration parameters. Sections were scored for variation in fibre size, loss of striation, hypereosinophilia, centralised nuclei and inflammation/inflammatory cells with a score of 0-3 (0-unaffected, 1-weak/present, 2-medium and 3-severe) with a potential maximum score of 15.

p-value for significance indicated as : ns= not significant.

Supplementary Figure 2. Sanger sequencing of DNA from whole blood from foetal liver chimeric mice.

Genotypes as indicated in the chromatograms from Sanger sequencing. All chimeric mice showed the integration of corresponding foetal liver cells in the bone marrow. The arrow heads indicate base position Chr7:102421471. W= A>T.

Supplementary Figure 3. Relative quantification of the Stim1 cDNA levels by qPCR in whole blood.

Relative quantification of the *Stim1* cDNA levels by qPCR in whole blood showed a significant reduction in the mean level in heterozygous $Stim1^{+/R304W}$ mice (Het, n=19) compared with wildtype WT controls (n=5) (*=$p<0.05$).

References

[1] R.M. Luik, B. Wang, M. Prakriya, M.M. Wu, and R.S. Lewis, Oligomerization of STIM1 couples ER calcium depletion to CRAC channel activation, Nature 454 (2008) 538-542.

[2] M.M. Wu, R.M. Luik, and R.S. Lewis, Some assembly required: constructing the elementary units of store-operated Ca2+ entry, Cell Calcium 42 (2007) 163-172.

[3] J.W. Putney, Jr., A model for receptor-regulated calcium entry, Cell Calcium 7 (1986) 1-12.

[4] J.W. Putney, Jr., New molecular players in capacitative Ca2+ entry, J. Cell. Sci. 120 (2007) 1959-1965.

[5] S. Feske, Y. Gwack, M. Prakriya, S. Srikanth, S.H. Puppel, B. Tanasa, A mutation in Orai1 causes immune deficiency by abrogating CRAC channel function, Nature 441 (2006) 179-185.

[6] R.S. Lacruz, and S. Feske, Diseases caused by mutations in ORAI1 and STIM1, Ann. N. Y. Acad. Sci. 1356 (2015) 45-79.

[7] S. Feske, CRAC channelopathies, Pflugers Archiv : European journal of physiology 460 (2010) 417-435.

[8] J. Bohm, F. Chevessier, A. Maues De Paula, C. Koch, S. Attarian, C. Feger, Constitutive activation of the calcium sensor STIM1 causes tubular-aggregate myopathy, Am. J. Hum. Genet. 92 (2013) 271-278.

[9] D. Misceo, A. Holmgren, W.E. Louch, P.A. Holme, M. Mizobuchi, R.J. Morales, A dominant STIM1 mutation causes Stormorken syndrome, Hum. Mutat. 35 (2014) 556-564.

[10] Y. Endo, S. Noguchi, Y. Hara, Y.K. Hayashi, K. Motomura, S. Miyatake, Dominant mutations in ORAI1 cause tubular aggregate myopathy with hypocalcemia via constitutive activation of store-operated Ca(2)(+) channels, Hum. Mol. Genet. 24 (2015) 637-648.

[11] C. Picard, C.A. McCarl, A. Papolos, S. Khalil, K. Luthy, C. Hivroz, STIM1 mutation associated with a syndrome of immunodeficiency and autoimmunity, N. Engl. J. Med. 360 (2009) 1971-1980.

[12] V. Nesin, G. Wiley, M. Kousi, E.C. Ong, T. Lehmann, D.J. Nicholl, Activating mutations in STIM1 and ORAI1 cause overlapping syndromes of tubular myopathy and congenital miosis, Proc. Natl. Acad. Sci. U S A 111 (2014) 4197-4202.

[13] S. Feske, ORAI1 and STIM1 deficiency in human and mice: roles of store-operated Ca2+ entry in the immune system and beyond, Immunol. Rev. 231 (2009) 189-209.

[14] J. Stiber, A. Hawkins, Z.S. Zhang, S. Wang, J. Burch, V. Graham, STIM1 signalling controls store-operated calcium entry required for development and contractile function in skeletal muscle, Nat. Cell. Biol. 10 (2008) 688-697.

[15] Y. Baba, K. Nishida, Y. Fujii, T. Hirano, M. Hikida, and T. Kurosaki, Essential function for the calcium sensor STIM1 in mast cell activation and anaphylactic responses, Nat. Immunol. 9 (2008) 81-88.

[16] J. Bohm, F. Chevessier, C. Koch, G.A. Peche, M. Mora, L. Morandi, Clinical, histological and genetic characterisation of patients with tubular aggregate myopathy caused by mutations in STIM1, J. Med. Genet. 51 (2014) 824-833.

[17] J. Grosse, A. Braun, D. Varga-Szabo, N. Beyersdorf, B. Schneider, L. Zeitlmann, An EF hand mutation in Stim1 causes premature platelet activation and bleeding in mice, J. Clin. Invest. 117 (2007) 3540-3550.

[18] G. Morin, N.O. Bruechle, A.R. Singh, C. Knopp, G. Jedraszak, M. Elbracht, Gain-of-Function Mutation in STIM1 (P.R304W) Is Associated with Stormorken Syndrome, Hum. Mutat. 35 (2014) 1221-1232.

[19] T. Markello, D. Chen, J.Y. Kwan, I. Horkayne-Szakaly, A. Morrison, O. Simakova, York platelet syndrome is a CRAC channelopathy due to gain-of-function mutations in STIM1, Mol. Genet. Metab. 114 (2015) 474-482.

[20] H. Stormorken, O. Sjaastad, A. Langslet, I. Sulg, K. Egge, and J. Diderichsen, A new syndrome: thrombocytopathia, muscle fatigue, asplenia, miosis, migraine, dyslexia and ichthyosis, Clin. Genet. 28 (1985) 367-374.

[21] E. Harris, U. Burki, C. Marini-Bettolo, M. Neri, C. Scotton, J. Hudson, Complex phenotypes associated with STIM1 mutations in both coiled coil and EF-hand domains, Neuromuscul. Disord. (2017).

[22] K. Tamura, J. Dudley, M. Nei, and S. Kumar, MEGA4: Molecular Evolutionary Genetics Analysis (MEGA) software version 4.0, Mol. Biol. Evol. 24 (2007) 1596-1599.

[23] H. Li, and R. Durbin, Fast and accurate short read alignment with Burrows-Wheeler transform, Bioinformatics 25 (2009) 1754-1760.

[24] H. Li, B. Handsaker, A. Wysoker, T. Fennell, J. Ruan, N. Homer, The Sequence Alignment/Map format and SAMtools, Bioinformatics 25 (2009) 2078-2079.

[25] T. Rausch, T. Zichner, A. Schlattl, A.M. Stutz, V. Benes, and J.O. Korbel, DELLY: structural variant discovery by integrated paired-end and split-read analysis, Bioinformatics 28 (2012) i333-i339.

[26] K. Chen, J.W. Wallis, M.D. McLellan, D.E. Larson, J.M. Kalicki, C.S. Pohl, BreakDancer: an algorithm for high-resolution mapping of genomic structural variation, Nat. Methods. 6 (2009) 677-681.

[27] H. Li, A statistical framework for SNP calling, mutation discovery, association mapping and population genetical parameter estimation from sequencing data, Bioinformatics 27 (2011) 2987-2993.

[28] H. Thorvaldsdottir, J.T. Robinson, and J.P. Mesirov, Integrative Genomics Viewer (IGV): high-performance genomics data visualization and exploration, Brief Bioinform. 14 (2013) 178-192.

[29] J.A. Krawiec, H. Chen, S. Alom-Ruiz, and M. Jaye, Modified PAXgene method allows for isolation of high-integrity total RNA from microlitre volumes of mouse whole blood, Lab. Anim. 43 (2009) 394-398.

[30] J. Schindelin, I. Arganda-Carreras, E. Frise, V. Kaynig, M. Longair, T. Pietzsch, Fiji: an open-source platform for biological-image analysis, Nat. Methods 9 (2012) 676-682.

[31] C.F.A. Culling, R.T. Allison, and W.T. Barr, (1985) 21 - Hard tissue, In Cellular Pathology Technique (Fourth Edition). (Butterworth-Heinemann), pp 408-430.

[32] A.J. Cheng, and H. Westerblad, Mechanical isolation, and measurement of force and myoplasmic free [Ca(2+)] in fully intact single skeletal muscle fibers, Nat. Protoc. 12 (2017) 1763-1776.

[33] F.H. Andrade, M.B. Reid, D.G. Allen, and H. Westerblad, Effect of hydrogen peroxide and dithiothreitol on contractile function of single skeletal muscle fibres from the mouse, J. Physiol. 509 (Pt 2) (1998) 565-575.

[34] T.J. Hallam, and T.J. Rink, Agonists stimulate divalent cation channels in the plasma membrane of human platelets, FEBS Lett. 186 (1985) 175-179.

[35] W. Bergmeier, M. Oh-Hora, C.A. McCarl, R.C. Roden, P.F. Bray, and S. Feske, R93W mutation in Orai1 causes impaired calcium influx in platelets, Blood 113 (2009) 675-678.

[36] F. Ahmad, Y. Boulaftali, T.K. Greene, T.D. Ouellette, M. Poncz, S. Feske, Relative contributions of stromal interaction molecule 1 and CalDAG-GEFI to calcium-dependent platelet activation and thrombosis, J. Thromb. Haemost. 9 (2011) 2077-2086.

[37] R.H. Lee, R. Piatt, P.B. Conley, and W. Bergmeier, Effects of ibrutinib treatment on murine platelet function during inflammation and in primary hemostasis, Haematologica 102 (2017) e89-e92.

[38] I.D. Carbery, D. Ji, A. Harrington, V. Brown, E.J. Weinstein, L. Liaw, Targeted genome modification in mice using zinc-finger nucleases, Genetics 186 (2010) 451-459.

[39] A.R. Concepcion, M. Vaeth, L.E. Wagner, 2nd, M. Eckstein, L. Hecht, J. Yang, Store-operated Ca2+ entry regulates Ca2+-activated chloride channels and eccrine sweat gland function, J. Clin. Invest. 126 (2016) 4303-4318.

[40] S. Mancarella, S. Potireddy, Y. Wang, H. Gao, R.K. Gandhirajan, M. Autieri, Targeted STIM deletion impairs calcium homeostasis, NFAT activation, and growth of smooth muscle, FASEB J. 27 (2013) 893-906.

[41] D. Varga-Szabo, A. Braun, C. Kleinschnitz, M. Bender, I. Pleines, M. Pham, The calcium sensor STIM1 is an essential mediator of arterial thrombosis and ischemic brain infarction, J. Exp. Med. 205 (2008) 1583-1591.

[42] B. Turgeon, and S. Meloche, Interpreting neonatal lethal phenotypes in mouse mutants: insights into gene function and human diseases, Physiol. Rev. 89 (2009) 1-26.

[43] T. Li, E.A. Finch, V. Graham, Z.S. Zhang, J.D. Ding, J. Burch, STIM1-Ca(2+) signaling is required for the hypertrophic growth of skeletal muscle in mice, Mol. Cell. Biol. 32 (2012) 3009-3017.

[44] C.H. Cho, J.S. Woo, C.F. Perez, and E.H. Lee, A focus on extracellular Ca(2+) entry into skeletal muscle, Exp. Mol. Med. 49 (2017) e378.

[45] M.K. Tu, J.B. Levin, A.M. Hamilton, and L.N. Borodinsky, Calcium signaling in skeletal muscle development, maintenance and regeneration, Cell Calcium 59 (2016) 91-97.

[46] M. Seth, T. Li, V. Graham, J. Burch, E. Finch, J.A. Stiber, Dynamic regulation of sarcoplasmic reticulum Ca(2+) stores by stromal interaction molecule 1 and sarcolipin during muscle differentiation, Dev. Dyn. 241 (2012) 639-647.

[47] C.A. McCarl, C. Picard, S. Khalil, T. Kawasaki, J. Rother, A. Papolos, ORAI1 deficiency and lack of store-operated Ca2+ entry cause immunodeficiency, myopathy, and ectodermal dysplasia, J. Allergy Clin. Immunol. 124 (2009) 1311-1318 e1317.

[48] A.J. Cheng, N. Place, and H. Westerblad, Molecular Basis for Exercise-Induced Fatigue: The Importance of Strictly Controlled Cellular Ca(2+) Handling, Cold Spring Harb. Perspect. Med. 8 (2018).

A) Representative images of embryos at 15.5 dpc

B) HE stained sections of embryos at 16.5 dpc

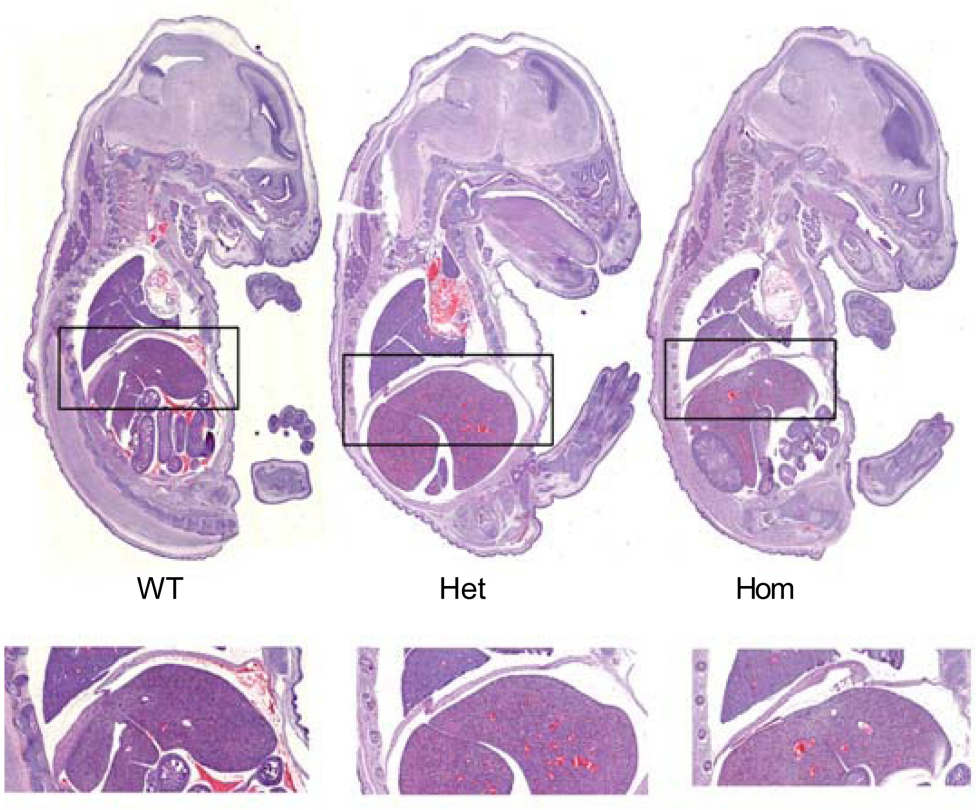

C) Platelet fraction in embryos (E15-E18)

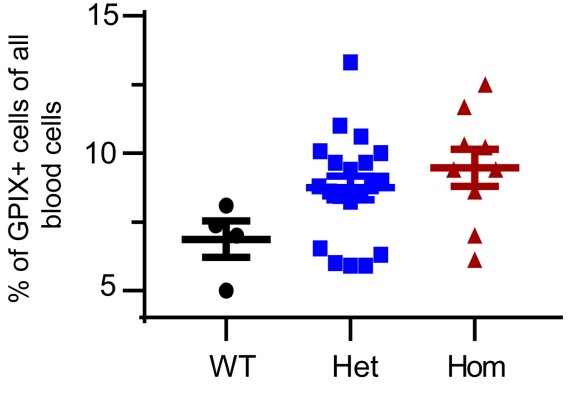

A) STIM1 ICH in adult paw skin

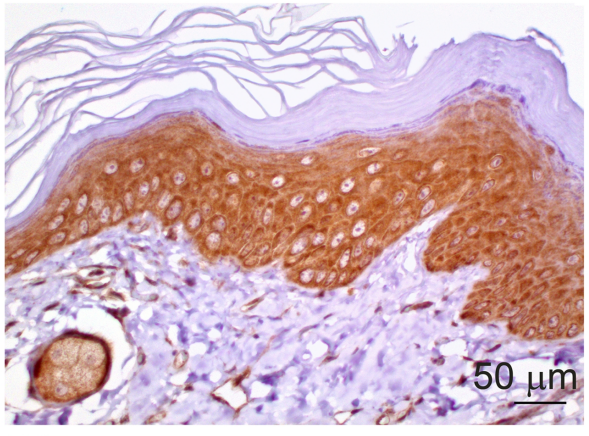

WT

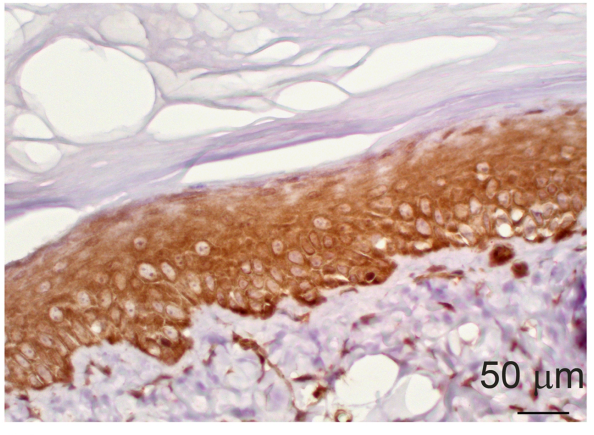

Hom

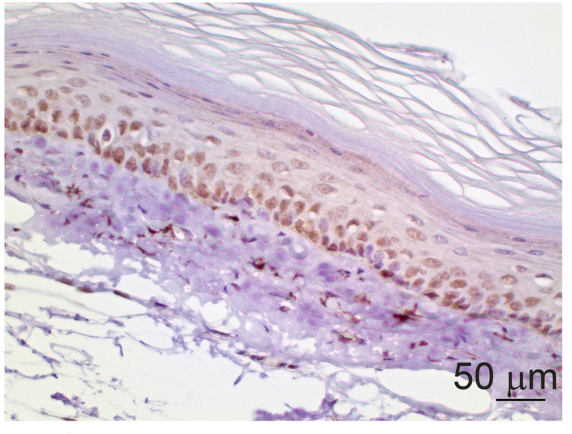

DKO

B) STIM1 IF in whole mount Hom embryos at 16.5 dpc

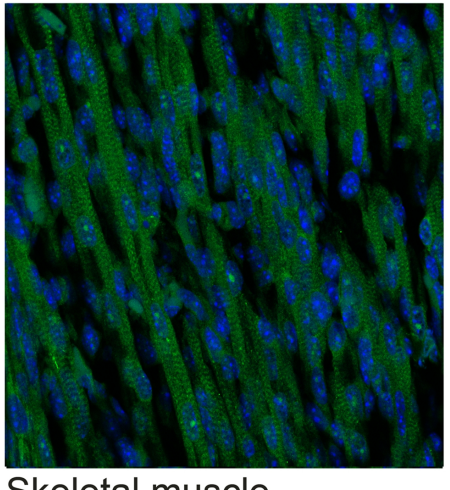

Skeletal muscle

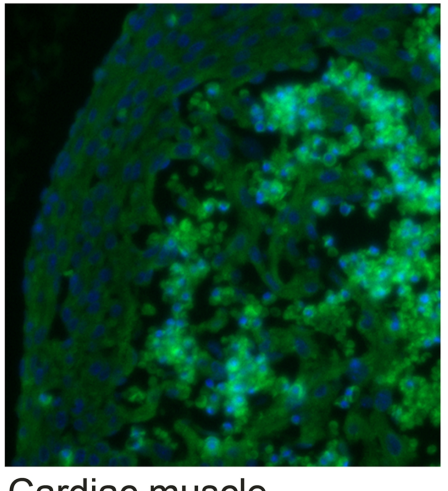

Cardiac muscle

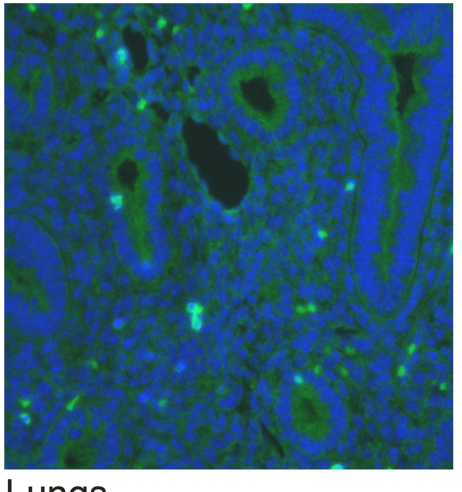

Lungs

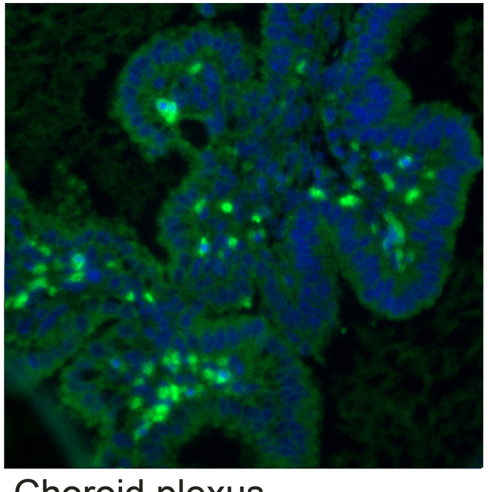

Choroid plexus

A-B) Whole cell Ca^{2+} measurements in mouse and human fibroblasts

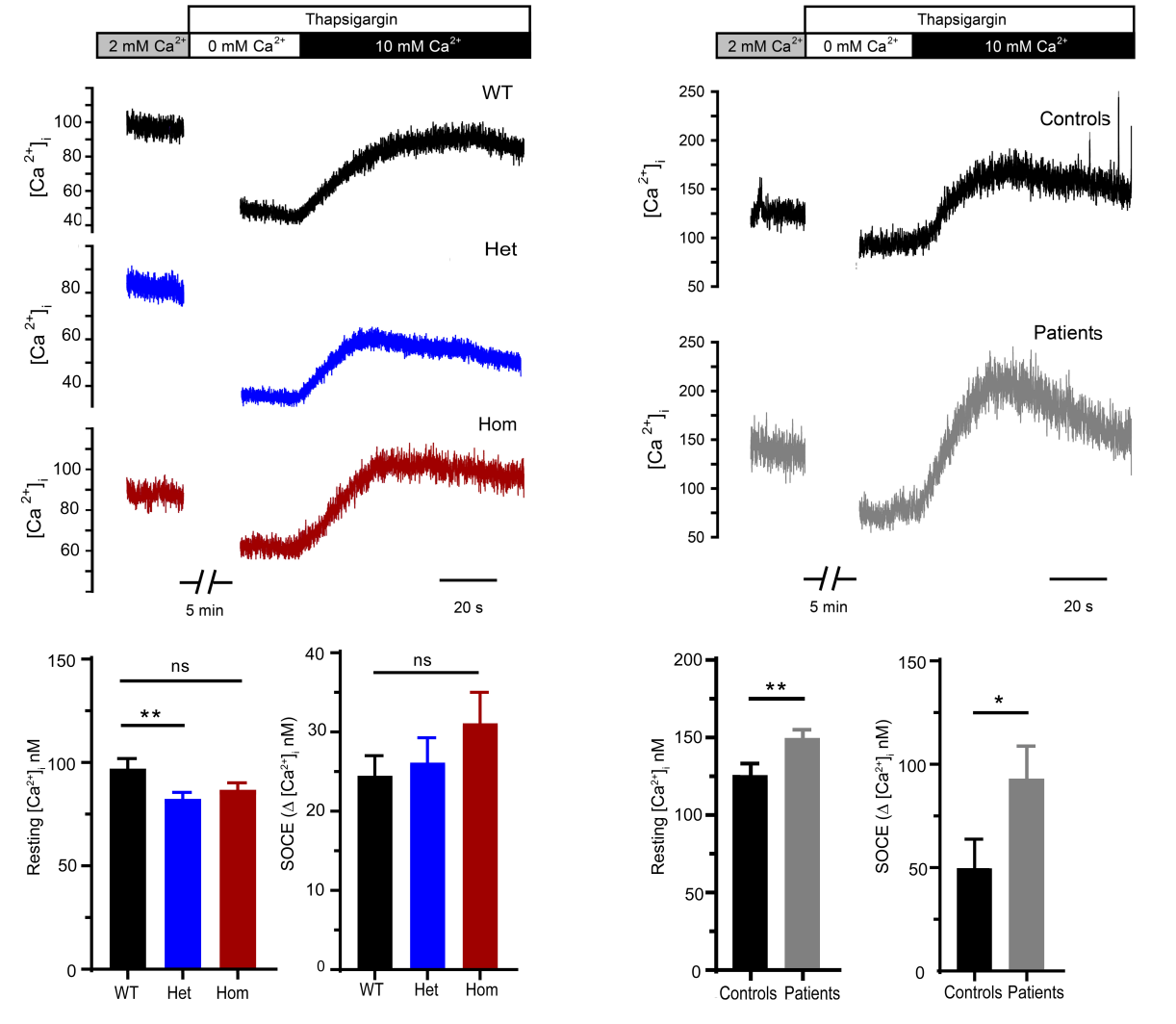

C) STIM1 in neonatal mouse fibroblasts

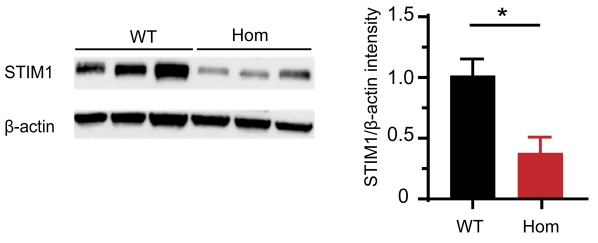

D) STIM1 in human fibroblasts

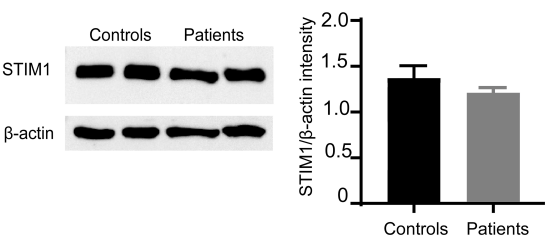

E) STIM1 activation and aggregation

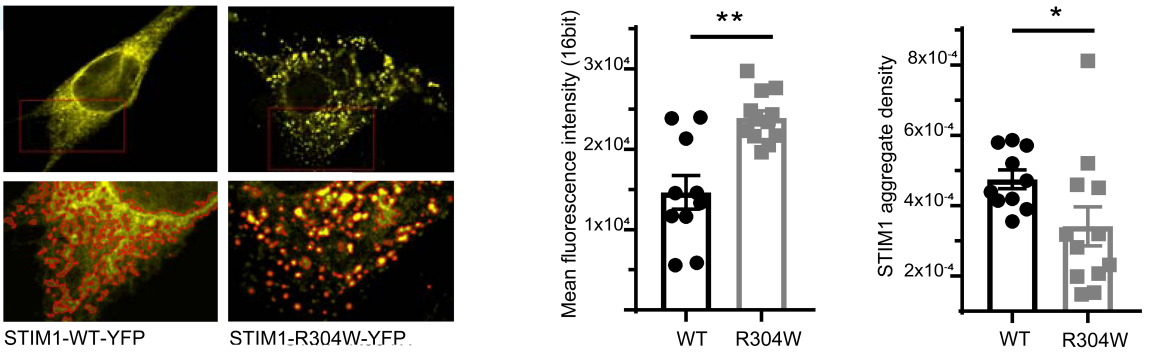

A) Body size

B) Growth curve of females

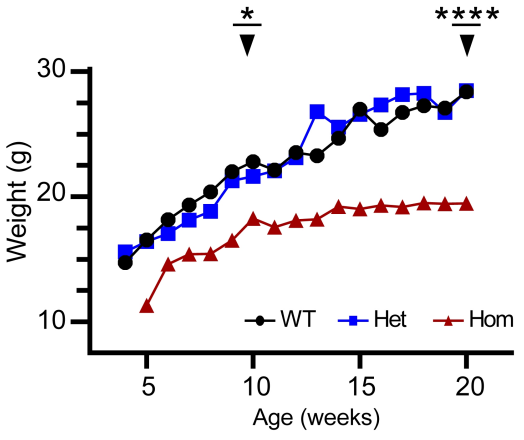

C) Reduced muscle mass

D) Excercise endurance

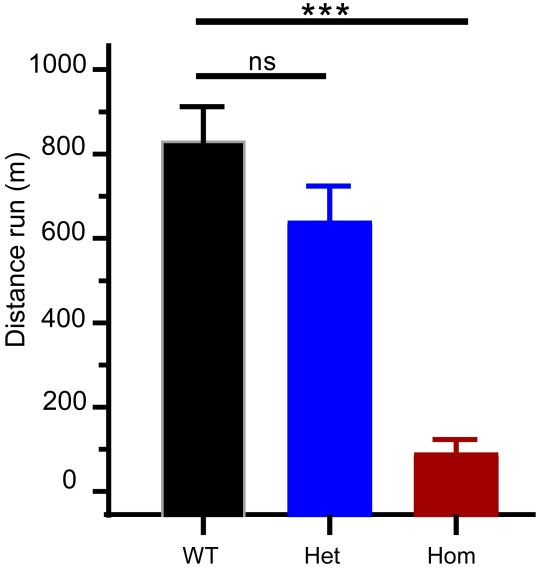

A) HE of WT quadriceps

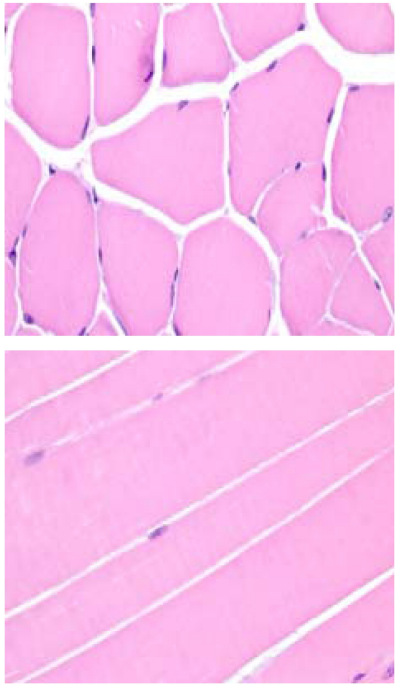

B) HE of Hom quadriceps

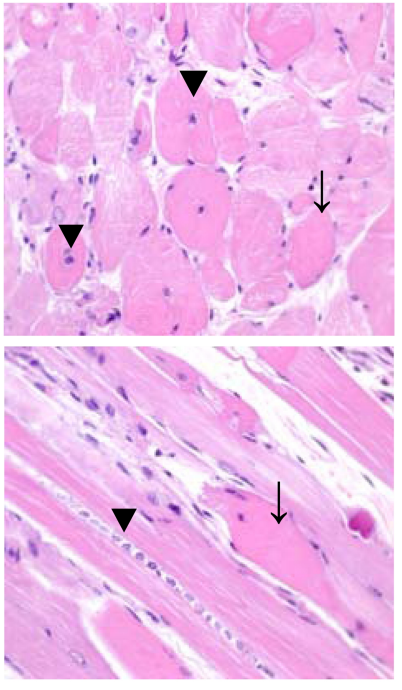

C) Severity score of degeneration in quadriceps

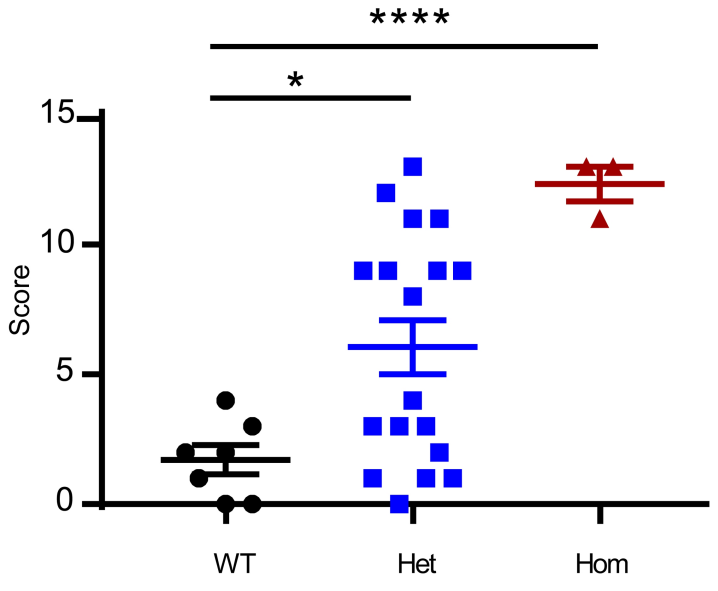

D) STIM1 IHC in WT

E) STIM1 IHC in Hom

F) Western blot for STIM1 in skeletal muscle

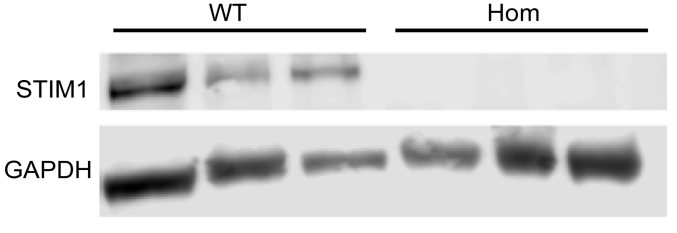

A) Tetanic $[Ca^{2+}]_i$-frequency relationship in FDB fibres

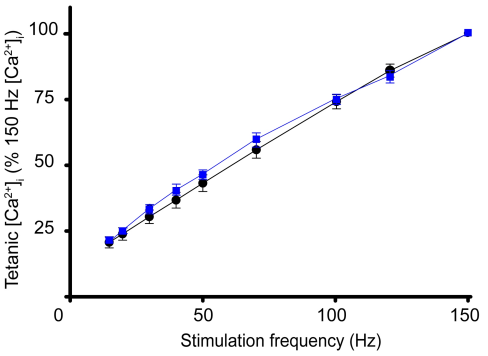

B) Tetanic force-frequency relationship in FDB fibres

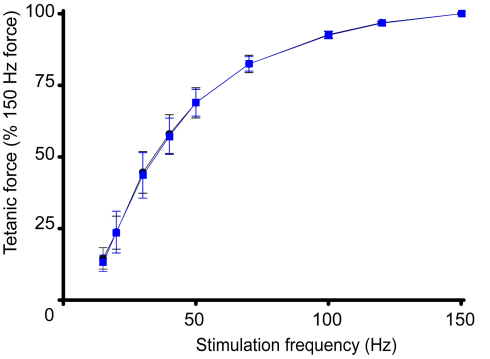

C) Average $[Ca^{2+}]_i$ during 70 Hz tetani

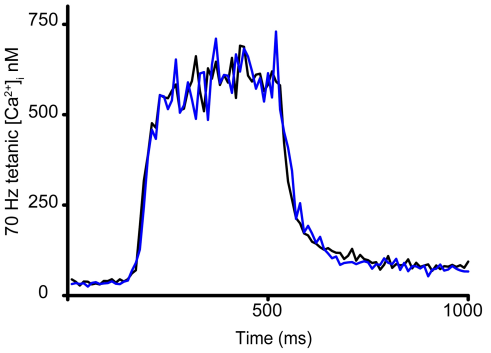

D) Average force during 70 Hz tetani

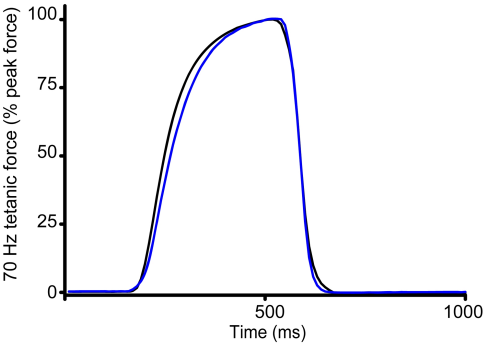

E-G) $[Ca^{2+}]_i$ and tetanic force in FDB fibres befeore and after fatigue

E)

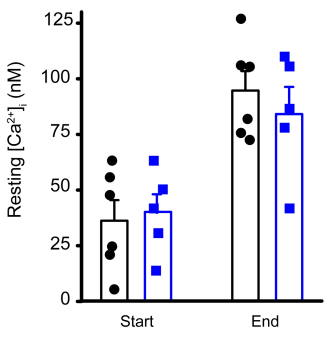

F)

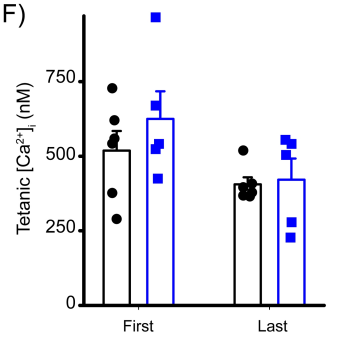

G)

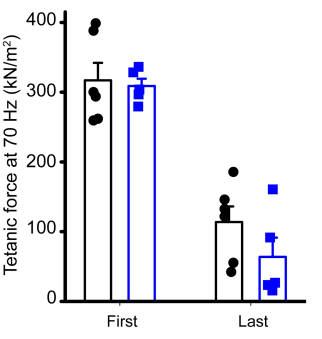

H) Indo-1 signal during Mn^{2+} quench indicating SOCE

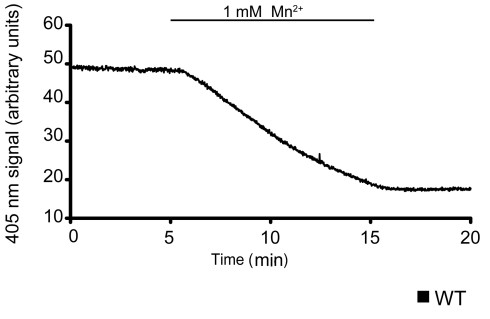

I) Mn^{2+} quench rate in FDB fibres

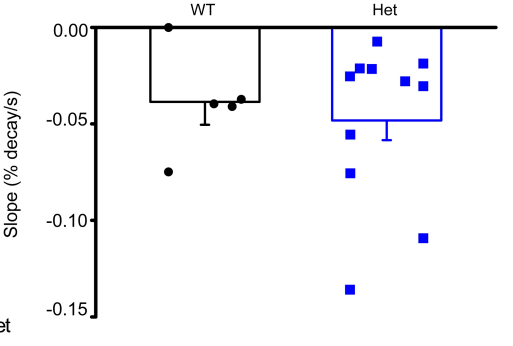

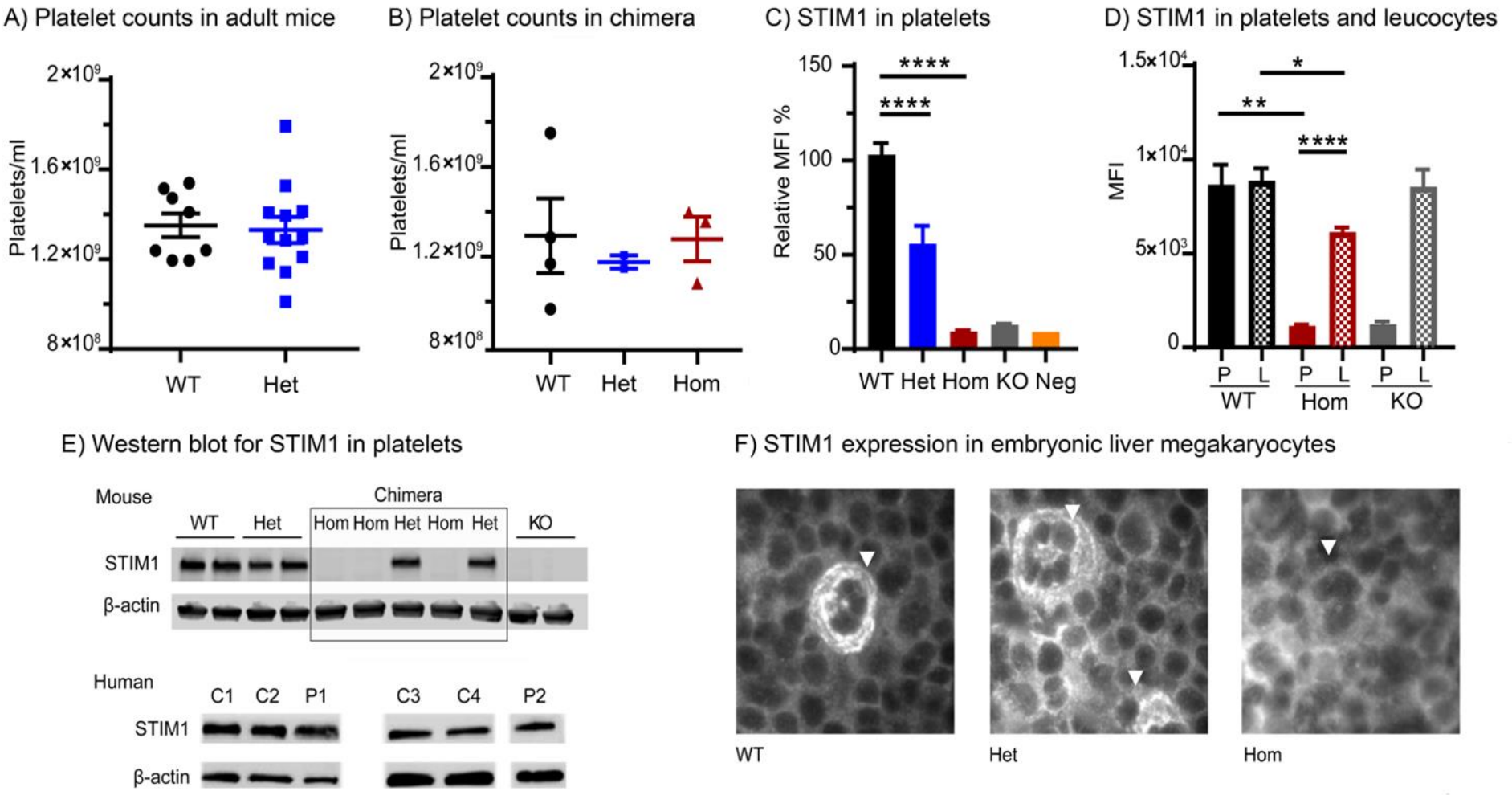
A) Platelet counts in adult mice
Platelets/ml
2×10⁹
1.6×10⁹
1.2×10⁹
8×10⁸
WT
Het
B) Platelet counts in chimera
Platelets/ml
2×10⁹
1.6×10⁹
1.2×10⁹
8×10⁸
WT
Het
Hom
C) STIM1 in platelets
Relative MFI %
150
100
50
0
****
****
WT Het Hom KO Neg
D) STIM1 in platelets and leucocytes
MFI
1.5×10⁴
1×10⁴
5×10³
0
*
**
****
P L
WT
P L
Hom
P L
KO
E) Western blot for STIM1 in platelets
Mouse
Chimera
WT
Het
Hom Hom Het Hom Het
KO
STIM1
β-actin
Human
C1 C2 P1
C3 C4 P2
STIM1
β-actin
F) STIM1 expression in embryonic liver megakaryocytes
WT
Het
Hom

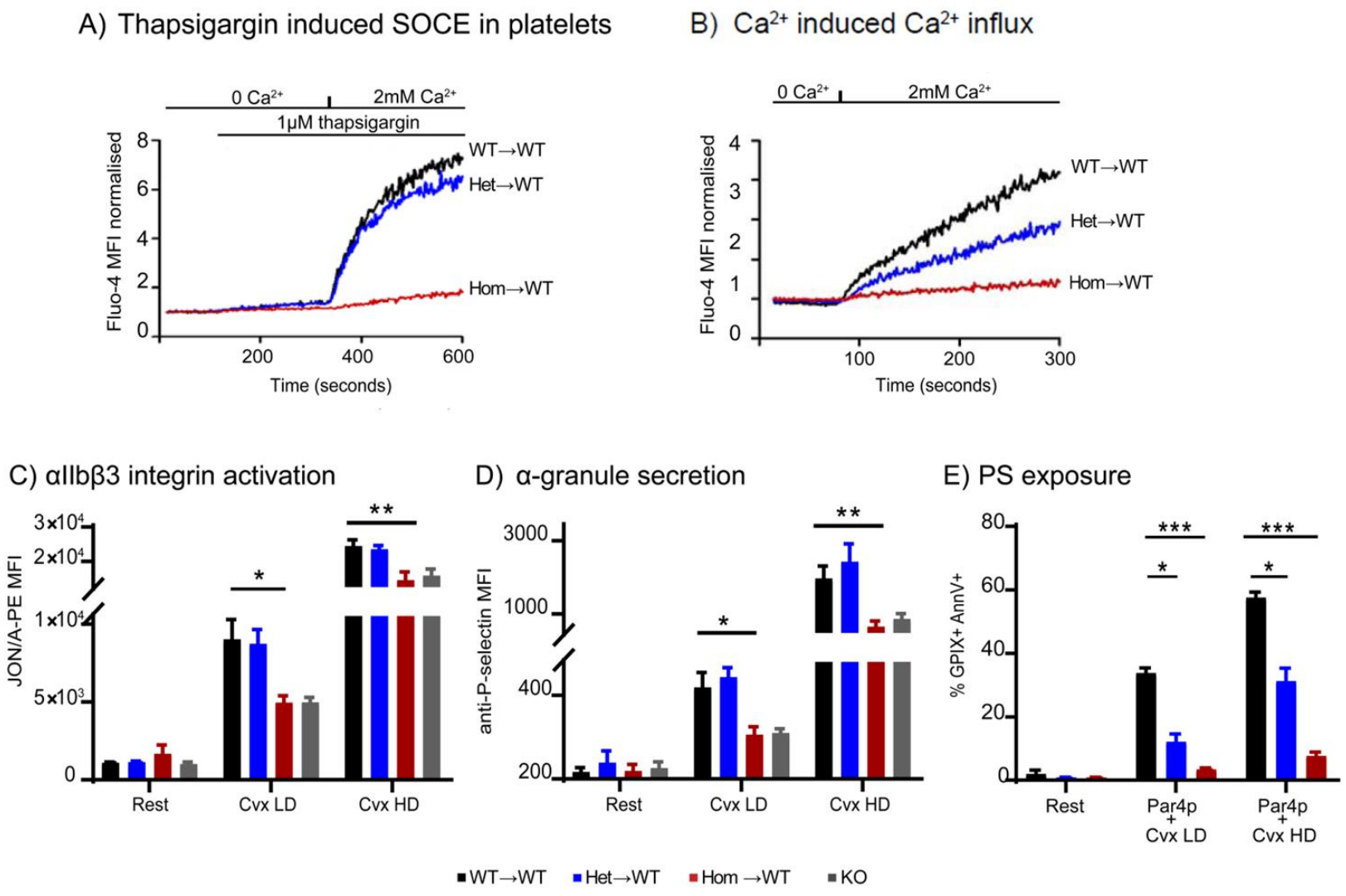
A) Thapsigargin induced SOCE in platelets
0 Ca2+
2mM Ca2+
1μM thapsigargin
Fluo-4 MFI normalised
Time (seconds)
WT→WT
Het→WT
Hom→WT
B) Ca2+ induced Ca2+ influx
C) αIIbβ3 integrin activation
JON/A-PE MFI
D) α-granule secretion
anti-P-selectin MFI
E) PS exposure
% GPIX+ AnnV+
Rest
Cvx LD
Cvx HD
Par4p + Cvx LD
Par4p + Cvx HD
KO

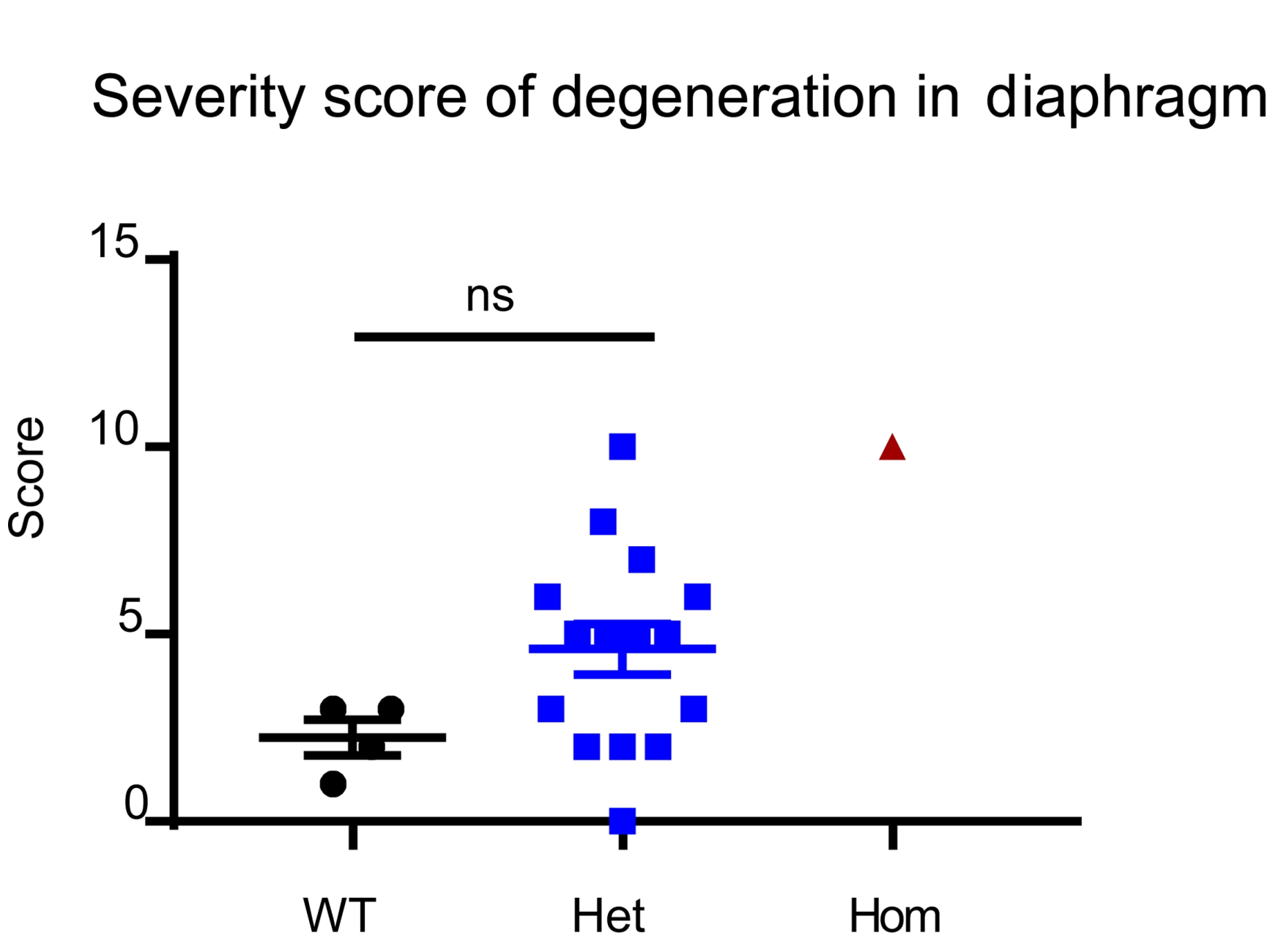
Severity score of degeneration in diaphragm
15
10
5
0
Score
ns
WT
Het
Hom

Sanger sequencing of whole blood drived DNA from foetal liver chimeric mice.

WT→WT DNA

WT chimera 1

C T G A G G G AGGGTAC

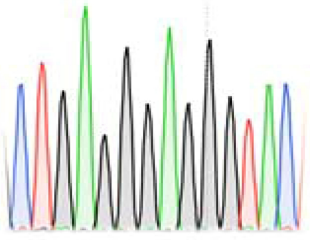

WT chimera 2

C T G A G G G AGGGTAC

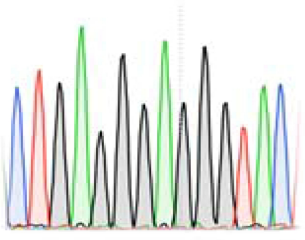

Het→WT DNA

Het chimera 1

C T G W G G G AGGGTAC

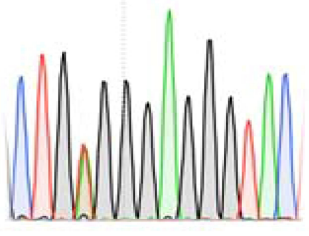

Het chimera 2

C TGWG G G AGGGTAC

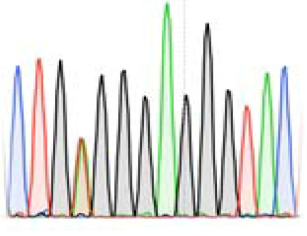

Hom→WT DNA

Hom chimera 1

C T G TG G G AGGGTAC

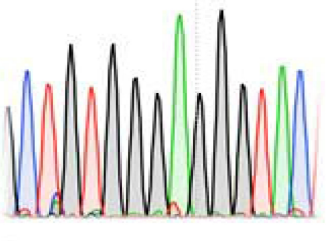

Hom chimera 2

C T G TG G G AGGGTAC

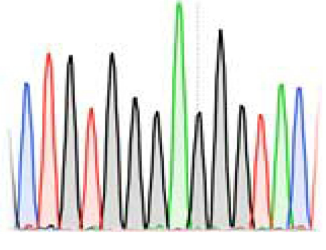

Hom chimera 3

C T G TG G G AGGGTAC

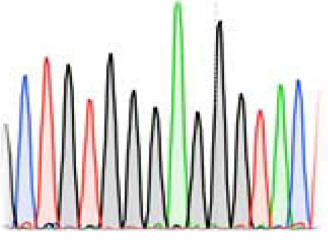

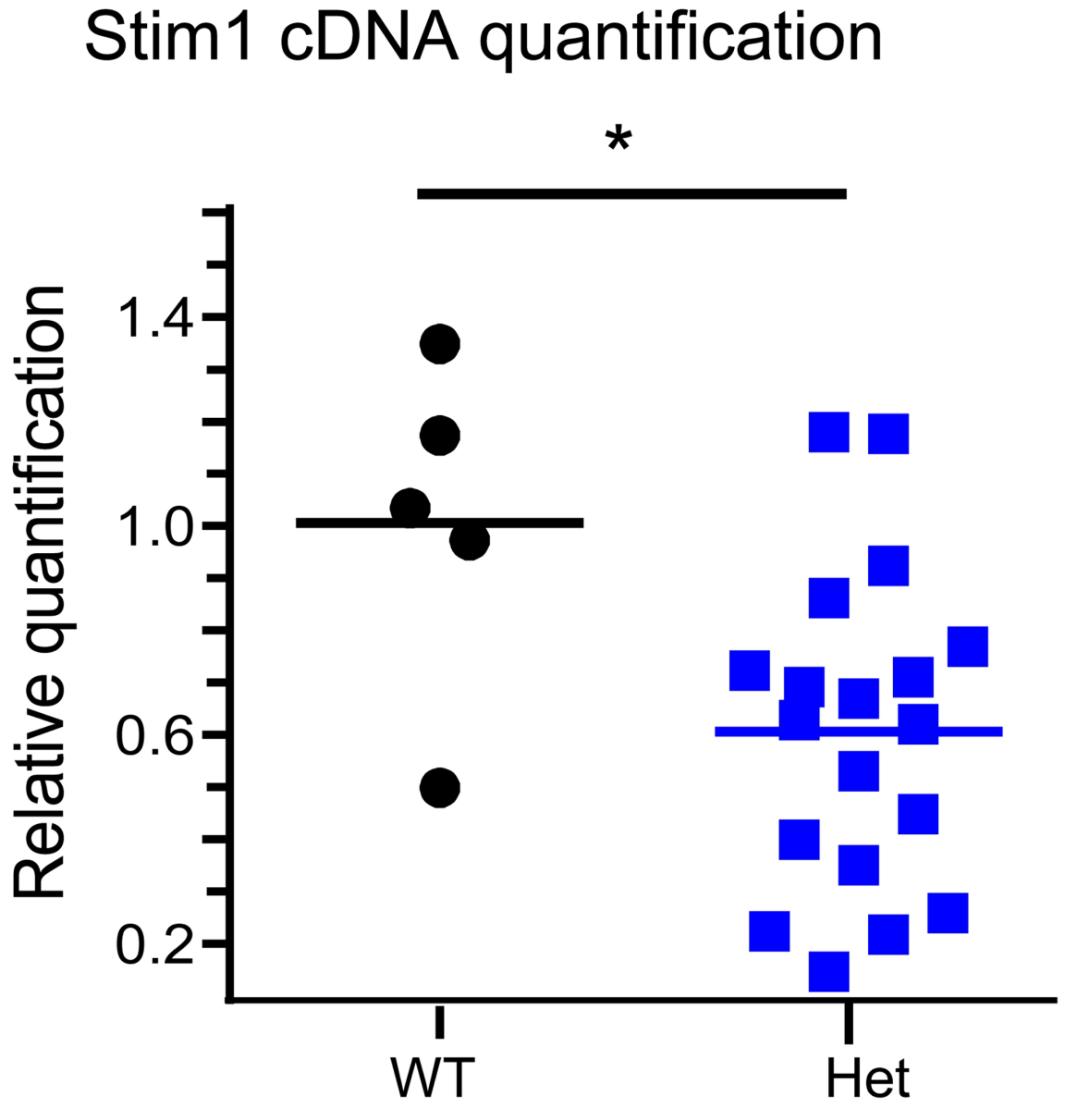
Stim1 cDNA quantification
*
Relative quantification
1.4
1.0
0.6
0.2
WT
Het

Supplementary Table 1

Primer name	Primer seq 5'-->3'	Chromosome location
Stim1 -F1	ATTGGTTTCTGTTGGCCCTGA	chr7:102421168
Stim1-R1	CCCCTTACCTGCCATTCTTTGA	chr7:102421695
Stim1-F2	CTCACCTGGACCTGAACCAT	chr7:102420366
Stim1-R2	GCTGCCAGAAGGAAAACAAG	chr7:102422512
Stim1-F3	GAGCACCGAACTGTGGAAGT	chr7:102421372
Stim1-R3	ATCCTCTGCCCTTTACGCAC	chr7:102421560
Stim1-R4	CCCACCAACCATTCAGAGTC	chr7:102422341
Stim1-R5	CCCTTCCCCTGACTGTGTAG	chr7:102420620
Stim1-R6	TCTTTCCATCCCCACTGCCA	chr7:102421927
Stim1_cDNA_F	gtggaagaaagtgatgagTTCCTAA	chr7:102354614-102408381
Stim1_cDNA_R	cagtccagttgtacaCTTCTGATGA	
Rplp0_cDNA_control1F	AGATTCGGGATATGCTGTTGGC	chr5:115560976-115561178
Rplp0_cDNA_control1R	TCGGGTCCTAGACCAGTGTTC	
Eef2_cDNA_control2F	TGGCCAAGTTTGCAGCCAAG	chr10:81179166-81179359
Eef2_cDNA_control2R	CCGGATCAAAGTACCGGTCTCC	
PPIB_control3f	CCAGGGCGGAGACTTCACCAGG	chr9:66063045-66065559
PPIB_control3r	CTCACCCAGCCAGGCCCGTA	

Supplementary Table 2

Antibody name/ Antibody registry code	Provider and catalog number	Concentration	Method	Dilution
STIM1-C terminal/NA	Gift (Stefen Feske, NYU, USA)	5 µg/µl	WB/IHC	1:1000
STIM1-C terminal/ AB_10738450	Sigma Aldrich S6197	1 mg/ml	IF	1:200
STIM1-N terminal/NA	LSBio LS-B10807	1mg/ml	FC	1:200
JON/A-PE/NA	Emfret analytics M023-2		FC	2 ug/ml
α-P selectin-FITC (Clone RB40.34 (RUO))/ AB_10896149	BD Biosciences 561923	0.5 mg/ml	FC	2 ug/ml
GPIX (clone Xia-B4) /NA	Emfret analytic M051-1		FC	2 ug/ml
PE Annexin V 200 tests/NA	BD Pharmingen 556421		FC	
β-actin/ AB_2242334	Cell Signaling Technology 3700S		WB	1:1000
Alexa Fluor 488 goat anti-mouse IgM/ AB_2633275	Thermo Fisher Scientific A32723	2 mg/ml	IF	1:200
Alexa Fluor 488 goat anti-mouse IgG1/ AB_2535764	Thermo Fisher Scientific A-21121	2 mg/ml	IF	1:200
Alexa Fluor 594 goat anti-rabbit IgG/AB_2534079	Thermo Fisher Scientific A-11012	2 mg/ml	IF	1:200
Anti-Rabbit IgG HRP conjugate/NA	Cell Signalling #7074		WB	1:1000
Anti-mouse IgM+IgG+IgA (H+L) HRP conjugate/ AB_2728714	SouthernBiotech 1010-05		WB	1:1000

Legend: IF=Immunofluorescence; IHC= Immunohistochemistry; WB= Western blot.

Supplementary Table 3

Chi-square test showed a significant deviation from the expected Mendelian ratio in the Stim1R304W live animals.

Expected n= 8 pups*25 crosses= 200 mice

Observed n= 130 mice

Outcome of 25 crosses $Stim1^{+/R304W}$ X $Stim1^{+/R304W}$

Genotype	Expected (n)	Observed (n)	Expected (%)	Observed (%)
$Stim1^{+/+}$	32.5	36	25	27.69
$Stim1^{+/R304W}$	65	91	50	70
$Stim1^{R304W/R304W}$	32.5	3	25	2.308
Total	**130**	**130**	**100**	**100**

Chi-square test	
Chi-square	37.55
Degree of freedom (DF)	2
P value (two-tailed)	0.0001
P value summary	****
Is discrepancy significant (P < 0.05)?	Yes

Supplementary Table 4

Chi-square test showed no deviations from the expected Mendelian ratio in Stim1R304W embryos observed *in utero*.

Expected n= 8 pups*14 crosses= 112 embryos

Observed n=92 embryos

Outcome of 14 crosses $Stim1^{+/R304W}$ X $Stim1^{+/R304W}$

Genotype	Expected (n)	Observed (n)	Expected (%)	Observed (%)
$Stim1^{+/+}$	23	20	25	21.74
$Stim1^{+/R304W}$	46	53	50	57.61
$Stim1^{R304W/R304W}$	23	19	25	20.65
Total	**92**	**92**	**100**	**100**

Chi-square test	
Chi-square	2.152
Degree of freedom (DF)	2
P value (two-tailed)	0.3409
P value summary ns	ns
Is discrepancy significant (P < 0.05)?	No